Molecular Psychiatry (2016) 21, 1573–1588

www.nature.com/mp

ORIGINAL ARTICLE

Predicting the functional states of human iPSC-derived neurons with single-cell RNA-seq and electrophysiology

C Bardy[1,2], M van den Hurk[1,3,7], B Kakaradov[4,7], JA Erwin[1], BN Jaeger[1], RV Hernandez[1], T Eames[1], AA Paucar[1], M Gorris[1], C Marchand[1], R Jappelli[1], J Barron[1], AK Bryant[1], M Kellogg[1], RS Lasken[5], BPF Rutten[3], HWM Steinbusch[3], GW Yeo[4,6] and FH Gage[1]

Human neural progenitors derived from pluripotent stem cells develop into electrophysiologically active neurons at heterogeneous rates, which can confound disease-relevant discoveries in neurology and psychiatry. By combining patch clamping, morphological and transcriptome analysis on single-human neurons *in vitro*, we defined a continuum of poor to highly functional electrophysiological states of differentiated neurons. The strong correlations between action potentials, synaptic activity, dendritic complexity and gene expression highlight the importance of methods for isolating functionally comparable neurons for *in vitro* investigations of brain disorders. Although whole-cell electrophysiology is the gold standard for functional evaluation, it often lacks the scalability required for disease modeling studies. Here, we demonstrate a multimodal machine-learning strategy to identify new molecular features that predict the physiological states of single neurons, independently of the time spent *in vitro*. As further proof of concept, we selected one of the potential neurophysiological biomarkers identified in this study—GDAP1L1—to isolate highly functional live human neurons *in vitro*.

Molecular Psychiatry (2016) **21,** 1573–1588; doi:10.1038/mp.2016.158; published online 4 October 2016

INTRODUCTION

The unprecedented access to live neurons from patients via human-induced pluripotent stem cell (iPSC) models is revolutionizing medical research opportunities in neurology and psychiatry. The translational success of these models depends on the ability to recapitulate *in vitro* the complexity of functional human brain circuits. Rapidly growing technological advances, which build on decades of elegant investigations on neurodevelopmental processes in animal models,[1,2] offer a panoply of protocols to drive cellular fates towards neurons of particular neurotransmitter classes (for example, dopaminergic, serotonergic) and brain region identities (for example, cortical neurons, midbrain neurons, motor neurons).[3–7] Many important studies have also shown that electrophysiologically active neurons can be generated from iPSCs or fibroblast-direct conversion.[5,8–13] Despite the clear success of generating highly functional neurons, it is also evident that such human cultures often comprise neuronal populations of heterogeneous electrophysiological states.[14] Indeed, patch-clamping experiments have reported an important variability of functional maturity among cell lines, cell batches and even within the same culture dish.[15–17] Co-culture with astrocytes or lengthy periods of time spent in neuronal medium have been reported to increase neuronal maturity on average but may also increase tissue culture variability.[18] In addition, the length of time required to reach functional maturation significantly varies among numerous published reports from 3 weeks to more than 5 months.[18,19] Such wide ranges may depend on many technical aspects such as loose criteria defining maturity, discrepancies in tissue culture protocols, or inherent differences among batches of cells.[20] Patch clamping is the current gold standard to demonstrate the functionality of a neuronal culture. However, patch clamping is low throughput and provides information for only a handful of neurons selected from several hundreds of thousands of cells. This technical limitation precludes a thorough characterization of the functional maturity of the actual neurons used with a variety of read outs for identifying the particular traits of patients' cell lines (for example, biochemistry, morphology, cell survival). In this study, we demonstrate a strategy to define functional states of human neurons *in vitro*, independently of time spent in culture. We bridge the gap between electrophysiology and molecular profile by successfully combining patch clamping, morphology and RNA-seq on single human neurons (PatchSeq). Using a machine-learning classifier trained on our multimodal dataset, we reveal new biomarkers that efficiently predict which neurons are highly functional. These biomarkers allow for the functional classification of a large number of neurons without patch clamping and can be used to stratify functional heterogeneity.

MATERIAL AND METHODS

Human neuronal culture

Human dermal fibroblasts were reprogrammed into pluripotent cells with the four Yamanaka factors (Oct3/4, Sox2, Klf4 and c-Myc), either in a retroviral vector or a non-integrating Sendai viral vector. Human iPSCs and embryonic stem cells (ESCs) were differentiated into neural progenitor cells (NPCs) as previously described.[6] NPCs were expanded for 3–5 passages (split 1:2 or 1:3 per passage) and stored at − 80 °C. Then they were thawed

[1]Salk Institute for Biological Studies, Stanford Consortium for Regenerative Medicine, La Jolla, CA, USA; [2]SAHMRI Mind & Brain, Laboratory for Human Neurophysiology and Genetics, School of Medicine Flinders University, Adelaide, SA, Australia; [3]Division of Translational Neuroscience, Department of Psychiatry and Neuropsychology, Maastricht University, Maastricht, The Netherlands; [4]Department of Cellular and Molecular Medicine, University of California, San Diego, La Jolla, CA, USA; [5]J. Craig Venter Institute, La Jolla, CA, USA and [6]Department of Physiology, Yong Loo Lin School of Medicine, National University of Singapore and Molecular Engineering Laboratory, A*STAR, Singapore, Singapore. Correspondence: Dr C Bardy or Dr GW Yeo or Dr FH Gage, Salk Institute for Biological Studies, 10010 North Torrey Pines Road, La Jolla, CA 92037, USA.
E-mail: cedric.bardy@sahmri.com or geneyeo@ucsd.edu or gage@salk.edu
[7]These authors contributed equally to this work.
Received 22 April 2016; revised 23 June 2016; accepted 1 July 2016; published online 4 October 2016

and expanded for at least one more passage in neural progenitor medium (DMEM/F12 supplemented with FGF8, SHH, B27 and N2, without retinoic acid). Dissociated NPCs were directly plated on glass coverslips (Fisher Scientific, Pittsburgh, PA, USA; Cat. No. 12-545-80) coated with poly-ornithine (Sigma, St. Louis, MO, USA; Cat. No. P3655) and laminin (Invitrogen/Thermo Fisher Scientific, Waltham, MA, USA; Cat. No. 23017-015) in 24-well plates. Twenty-four hours later, the cells were switched gradually (half medium change) to neuronal medium: BrainPhys basal[13] supplemented with 1 × N2 (Gibco/Thermo Fisher Scientific, Waltham, MA, USA; Cat. No. 17502-048), 1 × B27 (Gibco/Thermo Fisher Scientific, Cat No. 17504-044), brain-derived neurotrophic factor (BDNF, 20 ng ml^{-1}; PeproTech, Rocky Hill, NJ, USA; Cat. No. 450-02), glia-derived neurotrophic factor (GDNF, 20 ng ml^{-1}; PeproTech, Cat No. 450-10), ascorbic acid (AA, 200 nM; Sigma, Cat No. A0278), dibutyryl cyclic AMP (cAMP, 1 mM Sigma, Cat No. D0627), and laminin (1 μg ml^{-1}; Invitrogen/Thermo Fisher Scientific, Cat No. 23017-015). Half of the neuronal medium was gently replaced two to three times a week. The plates were kept in a humidified incubator at 37 °C with 5% CO_2 and 21% O_2. The pH (~7.3–7.4) and the osmolarity (~300–305 mOsmol l^{-1}) of medium were maintained constant over time.

Patch clamping

For whole-cell patch-clamp recordings, individual coverslips were transferred into a heated recording chamber and continuously perfused (1 ml min^{-1}) with either BrainPhys basal medium or artificial cerebrospinal fluid (ACSF) bubbled with a mixture of CO_2 (5%) and O_2 (95%) and maintained at 25 °C. The composition of ACSF was adjusted to match the inorganic salt concentration and osmolarity of BrainPhys basal. ACSF contained (in mM) 121 NaCl, 4.2 KCl, 1.1 $CaCl_2$, 1 $MgSO_4$ (or 0.4 $MgSO_4$ and 0.3 MgCl), 29 $NaHCO_3$, 0.45 NaH_2PO_4-H_2O, 0.5 Na_2HPO_4 and 20 glucose (all chemicals from Sigma).

For single-cell patch-clamp electrophysiological recordings, we used a digidata 1440 A/ Multiclamp 700B and Clampex 10.3 (Molecular Devices, Sunnyvale, CA, USA). Patch electrodes were filled with internal solutions containing 130 mM K-gluconate, 6 mM KCl, 4 mM NaCl, 10 mM Na-HEPES, 0.2 mM K-EGTA; 0.3 mM GTP, 2 mM Mg-ATP, 0.2 mM cAMP, 10 mM D-glucose, 0.15% biocytin and 0.06% rhodamine. The pH and osmolarity of the internal solution were close to physiological conditions (pH 7.3, 290–300 mOsmol). Data were all corrected for liquid junction potentials (10 mV). Electrode capacitances were compensated on-line in cell-attached mode (~7 pF). Recordings were low-pass filtered at 2 kHz, digitized, and sampled at intervals of 50 ms (20 kHz). To control the quality and the stability of the recordings throughout the experiments, access resistance, capacitance and membrane resistance were continuously monitored on-line and recorded. The resistance of the patch pipettes was between 3 and 5 MOhm. The access resistance of the cells in our sample was ~40 MOhm on average. Spontaneous synaptic AMPA events were recorded at the reversal potential of Cl^- and could be reversibly blocked by AMPA receptor antagonist (10 μM NBQX, Sigma Ref#N183). Spontaneous synaptic GABA events were recorded at the reversal potential of cations and could be reversibly blocked with GABAa receptor antagonist (10 μM SR95531, Sigma Ref#S106). Statistical analysis of electrophysiology data was assisted with Clampfit 10.3 (pCLAMP Software suite, Molecular Devices, Sunnyvale, CA, USA), MATLAB 2014b (MathWorks, Natick, MA, USA), Igor Pro 6 (WaveMetrics, Lake Oswego, OR, USA), Prism 6 (GraphPad Software, La Jolla, CA, USA), Mini Analysis (Synaptosoft, Decatur, GA, USA), Excel (Microsoft Corporation, Redmond, WA, USA) and custom-made Python programs.

Electrophysiological recording protocol

The same electrophysiological protocol was applied to all neurons ($n = 290$). Whole-cell patch-clamp recordings were obtained in the absence of any receptor antagonists in ACSF or BrainPhys basal. After breaking the membrane seal, we first maintained the cell in voltage clamp (VC) at −70 mV by injecting small amounts of current when necessary ('Baseline at −70 mV'). We applied a test pulse of −5mV to measure passive cell properties (membrane resistance, access resistance, capacitance). Voltage-dependent sodium and potassium channels properties were examined with an IV curve. Spontaneous synaptic events mediated by AMPA receptors were recorded for at least 5 min at −70 mV (close to Cl^- reversal potential). The nature of AMPA synaptic events was confirmed on a small subset of cells ($n = 15$, excluded from RNA-seq) by reversible blockade with AMPA receptor antagonist (10 μM NBQX). The patch was then switched to current clamp. Small currents were injected if necessary to maintain the cell resting potential around −70 mV. Current steps (increments 2 pA, $n = 15$, 500 ms) were applied to measure the properties of evoked action potentials (APs). Next, spontaneous APs were recorded for 1–5 min at −70 mV and then at resting potential without injecting any current (CC 0 pA). The patch was then reversed to voltage clamp and slowly increased to the reversal potential of cations (~0 mV). Once the baseline stabilized, we recorded spontaneous gabaergic synaptic activity for 5–10 min. The nature of GABA synaptic events was confirmed on a small subset of cells ($n = 5$, excluded from RNA-seq) by reversible blockade with GABAa receptor antagonist (10 μM Gabazine).

AP Type classification

'Type 0 cells' did not express voltage-dependent sodium currents and were excluded from analysis. 'Type 1 neurons' expressed small Nav currents but were not able to fire APs above −10 mV. The arbitrary limit of −10 mV was chosen as it is close to the reversal potential of cations (0 mV). Healthy APs usually reach or overshoot the reversal potential of cations. 'Type 2 neurons' fired one AP above −10 mV, which was followed by a plateau. 'Type 3 neurons' also fired one AP above −10 mV and one or a few aborted spikes below −10 mV. 'Type 4 neurons' fired more than one AP above −10 mV but at a frequency below 10 Hz. 'Type 5 neurons' fired APs above −10 mV at 10 Hz or more. Our categorization of functional types of neurons followed a continuum that relates to the stage of maturity of the neurons. Although Type 1 neurons are considered immature, Type 5 neurons are considered more mature and functionally active. Although after ~3–6 weeks of maturation we found on average ~75% of Type 4–5 neurons, we found every ePhys type of cell at most differentiation time points we looked at (range of 2 weeks to 5 months after NPC maturation). This finding suggests some degree of variability in the electrophysiological maturity of neurons even within cultures of the same age. Remarkably, in our samples, the large majority of cells receiving active excitatory synapses were Type 5 neurons and we almost never found clear, spontaneously active AMPA and GABA synaptic inputs in Type 1 neurons and rarely in Type 2.

Neuromorphometry

Images of the patch-clamped cells were taken with a 40× water-immersion objective, differential interference contrast filters (all Olympus, Tokyo, Japan), an infrared digital camera (Rolera XR; QImaging, Surrey, BC, Canada), and an epifluorescence mercury lamp. Mosaics of the several fields of views to cover the span of the neurites were taken and stitched later on Neurolucida (MBF Bioscience, Williston, VT, USA). Before patch clamping, the targeted cells were imaged with DIC and epifluorescence (most cells patched expressed synapsin-GFP). The entire cells were filled with a red fluorescent dye (rhodamine) and another set of images was taken rapidly after completion of the electrophysiological recordings. All the images were stitched and analyzed on Neurolucida. The soma size and shape were measured on the DIC images before patching to avoid deformation by the patch pipette. The images from the intracellular rhodamine dye, occasionally supplemented by GFP vectors, were used to guide the neuromorphological reconstruction. For all cells, the morphology was reconstructed within a radius of 150 μm. Many cell processes reached beyond that distance but, for homogeneity of the sample, we restricted the analysis to that arbitrary radius. Occasionally, patched cells with pictures of insufficient quality were excluded from the analysis. When necessary, some processes partially hidden by the patch electrode were extrapolated.

Single-cell collection and cDNA preparation

Following electrophysiological recording, we applied slight additional negative pressure to establish a stronger connection between cell and patch electrode, but without completely aspirating the cell in the pipette. The neuron, including its processes (axon and dendrites), was then transferred in a volume of ~2 μl of internal patch solution into a PCR tube containing 8 μl sample buffer by slowly retracting the patch pipette from the chamber bath and breaking the tip of the electrode along the inside wall of the tube. Sample buffer was made according to the protocol supplied by Clontech with the SMARTer Ultra Low RNA Kit and included both ERCC spike-ins (Ambion/Thermo Fisher Scientific) and ArrayControl spikes 1, 4 and 7 (RNA standard for the Fluidigm C1) for the purpose of quality control (QC). Successful removal of the cell from the coverslip was always confirmed by DIC optics. Collected single cells were immediately spun down and put on ice for SMARTer cDNA synthesis following manufacturer's instructions (Clontech, Mountain View, CA, USA). Briefly, first-strand cDNA was synthesized from poly(A)+ RNA by incubation with 1 μl of 3′ SMART CDS Primer II A (24 μM) for 3 min at 72 °C, followed by

reverse transcription in a 20-µl final reaction volume using 200 units of SMARTScribe Reverse Transcriptase for 90 min at 42 °C and inactivation for 10 min at 70 °C. First-strand cDNA was then purified using Agencourt AMPure XP SPRI Beads (Beckman Coulter Genomics, Danvers, MA, USA) and amplified by long-distance PCR using the Advantage 2 PCR Kit (Clontech) with the following PCR thermocycler program: 95 °C for 1 min, 18 cycles of 95 °C for 15 s, 65 °C for 30 s, 68 °C for 6 min, and 72 °C for 10 min. PCR-amplified double-stranded (ds) cDNA was immobilized onto SPRI beads, purified by two washes in 80% ethanol, and eluted in 12 µl of purification buffer (Clontech). The quality (Agilent 2100 Bioanalyzer High Sensitivity DNA Kit; Agilent Technologies, Santa Clara, CA, USA) and quantity (Qubit dsDNA High Sensitivity Assay Kit; Invitrogen/Thermo Fisher Scientific) of each ds cDNA sample were assessed before library preparation.

qPCR assays

To select the single-cell cDNA samples suitable for mRNA-seq, we determined the level of expression of GAPDH and beta-actin (ACTB) in each sample by TaqMan real-time PCR. Samples with Ct values $\leqslant 30$ for both housekeeping genes were typically considered positive for library preparation. For each gene, duplicate 10-µl PCR reactions were performed on an ABI Prism 7900 Sequence Detector (Applied Biosystems/Thermo Fisher Scientific, Waltham, MA, USA) using 0.50 µl of 1:5-diluted ds cDNA template in standard TaqMan Gene Expression Assay with FAM reporter. Real-time PCR assays for detection of the ERCCs and ArrayControl RNA spikes were performed using, respectively, standard TaqMan Gene Expression Assays and SYBR Green PCR Master Mix (Thermo Fisher Scientific) with custom primers (Fluidigm, South San Francisco, CA, USA).

Illumina transcriptome library preparation and sequencing

Construction of single-cell mRNA-seq libraries was typically performed with 0.25 ng of input cDNA using the Nextera XT DNA sample prep kit (Illumina, San Diego, CA, USA) with modified protocol. Briefly, cDNA was tagmented for 5 min at 55 °C in a 5-µl reaction containing 2.5 µl of Tagment DNA Buffer and 1.25 µl of Amplicon Tagment Mix; tagmentation was neutralized with 1.25 µl of Neutralize Tagment Buffer for 5 min. Tagmented DNA was then subjected to 12-cycle PCR amplification using 3.75 µl of Nextera PCR Master Mix and 1.25 µl each of index 1 (i7) and index 2 (i5) library-identifying (barcoded) sequencing primers. The constructed libraries were run on a 1.5% agarose gel in Tris-borate/EDTA buffer, stained with SYBR Gold (Invitrogen), and size selected for ~300–400 or ~300–650 bp (insert size of ~165–265 or ~165–515 bp, respectively). Gel-excised library fragments were purified with the Wizard SV Gel and PCR Clean-Up System (Promega, Madison, WI, USA), eluted in 40 µl of nuclease-free water, and concentrated by speedvacuum centrifugation. Each library was then quantified (Qubit dsDNA High Sensitivity Assay Kit; Invitrogen/Thermo Fisher Scientific) and examined for correct size (Agilent 2200 TapeStation High Sensitivity D1K ScreenTape Assay; Agilent Technologies), after which equimolar amounts of uniquely barcoded libraries were pooled together and used for cluster generation and 100-bp paired-end sequencing on a HiSeq 2000 or 2500 sequencer (Illumina).

Bioinformatic analysis of single-cell transcriptomes

Single-cell mRNA sequencing data from $n = 56$ patched human neurons, which passed a series of QC, allowed us to correlate electrophysiological profiles with gene expression profiles. For each of $n = 56$ neurons, raw sequencing reads were mapped to the human reference transcriptome (Gencode v19) using gapped-alignment strategies. Alignment was performed by STAR (version 2.3.0) followed by gene-level quantification with HTseq (version 0.6.1). Per-gene expression outputs were scaled to transcripts per million (tpm) units.

Data transformation and dimensionality reduction for transcriptome principal component analysis

Whole-gene expression tpm counts were log-transformed: log(tpm+1) to normalize their distribution. Principal component analysis (PCA) was performed on the log-transformed expression matrix E (cells = rows, genes = columns). Before PCA dimensionality reduction, the expression of each gene (column) was standardized by subtracting the mean expression of that gene across all 56 cells and dividing by its s.d. All 56 cells were scatter-plotted against the first two principal components of the expression matrix E. Although the PCA of the transcriptomes was unsupervised, each cell was later colored on the plot by its respective AP Type, allowing us to visually assess any functionally significant clustering. To formalize this, we also performed hierarchical agglomerative clustering (Euclidean distance, average linkage) of the cell–cell covariance matrix (E*E′).

Differential expression between intermediate and functional neuron states

The five AP Types of differentiated neurons were stratified into immature (Types 1–3), transitional (Type 4) and highly functional (Type 5) neurons. To identify differentially expressed genes in these neuron groups, two non-parametric statistical tests were used: Mann–Whitney *U* (MWU) and Kolmogorov–Smirnoff 2-sided (KS2). The reported *P*-values are presented, but the threshold for significance is Bonferroni-corrected from $P < 0.05$ to $P < 3.1e-6$.

Extremely randomized trees classifier

The algorithm learned to classify the functional states of neurons solely based on their molecular phenotypes (gene expression). We stratified the cells into two classes based on electrophysiological states. The classifier randomly selected 90% of the cells in our sample for training. The testing was performed on the remaining 10%. To obtain a predictive value for each cell, we reiterated the learning phase 10 times. Using the extremely randomized trees classifier[21] with 10-fold cross-validation, we achieved good validation performance with >85% generalization accuracy, as shown by a high area under the receiver operating characteristic (ROC) curve (area under the curve = 0.93). The maximum number of features was 200, and we used 900 estimators.

Construction of GDAP1L1-EGFP lentiviral reporter vector

A transcriptional reporter lentivector encoding EGFP was designed to track human cells expressing gene GDAP1L1 (ganglioside-induced differentiation associated protein 1-like 1). A 1350 bp 5′ gene region—chr20:44,245,985-44,247,334—UCSC Human Genome Browser Dec. 2013 (GRCh38/hg38) Assembly, located precisely upstream to the gene's translation start codon and including a 77 bp 5′UTR, was used as a promoter. The sequence was amplified from male genomic DNA (Promega) with Phusion High-Fidelity DNA Polymerase (NEB) using the forward primer G220 (5′-CGTTATCG ATGTATGCTGAACCAGGGAGGCT), which adds a ClaI site, and the reverse primer G221 (5′-attactcgaggacagcccggaatcagaggca), which adds a *Xho*I site. The PCR product was introduced as a promoter into the lentiviral vector (LV) pCSC-Syn-mcs-EGFP, a derivative of pCSC-SP-PW-EGFP.[22] The construct (pCSC-GDAP1L1-EGFP) was verified by DNA sequencing.

Immunohistochemistry

Immunohistochemistry experiments were performed on neurons plated on glass coverslips. Standard immunohistochemistry protocols were used. Coverslips were stained with DAPI and a combination of the following antibodies: mouse-Map2(2a+2b) (1:500, Sigma), mouse-TUJ1 (1:1000; Covance, Princeton, NJ, USA), Rabbit-GFAP (1:200; Dako, Carpinteria, CA, USA) and GDAP1L1 (1:250; OriGene, Rockville, MD, USA).

Fluorescence-activated cell sorting analysis

Adherent neuronal cultures were thoroughly washed with DPBS without Mg^{+} and Ca^{+} before dissociating with Accutase containing DNAse (100 U ml^{-1}) for 5 min at room temperature. Cell suspensions were collected with DPBS containing 1% knockout serum replacement (KOSR) and spun down at 200 rfc for 5 min. The cell pellet was gently resuspended in DPBS containing 1% KOSR, 2 mM EDTA, and DNase (100 U ml^{-1}). Cell suspension was passed through a 70-µm nylon cell strainer and sorted using a Becton-Dickinson Influx cytometer (BD Biosciences, Franklin Lakes, NJ, USA). Gated samples were collected in 15-ml tubes containing BrainPhys-based neuronal differentiation medium containing Rho kinase (ROCK) inhibitor (STEMCELL Technologies, Vancouver, BC, Canada) and penicillin-streptomycin (Thermo Fisher Scientific). After sorting, we re-plated 50 000 neurons (GDAP1L1:eGFP-positive and GFAP:tdTomato negative) per well (48-well plate) on to poly-ornithine/laminin-coated 8-mm glass coverslips containing established human astrocytes-cerebellar (ScienCell Research Laboratories, Carlsbad, CA, USA) at 70% confluence. The medium was changed 24 h post-sort to BrainPhys differentiation medium without ROCK inhibitor, and the re-plated cells were cultured as previously described.[13]

Statistics

Unless specified clearly otherwise, throughout the manuscript we present the mean and standard error of the mean. Concerned to avoid the assumption of Gaussian distribution in our samples, we consistently used non-parametric statistics such as Spearman, Mann–Whitney and Wilcoxon. Statistics were two-tailed and Bonferroni-corrected for multiple hypotheses tests. In several plots, to estimate the goodness of fit of the linear regression represented graphically, we reported the R^2 and the corresponding *P*-values, which estimates how significantly the slope deviates from zero.

RESULTS

Human neuronal circuits were established *in vitro* from iPSCs and ESCs (H9 line) (Figure 1a). IPSCs were reprogrammed from the fibroblast cells of four healthy individuals. IPSCs and ESCs were

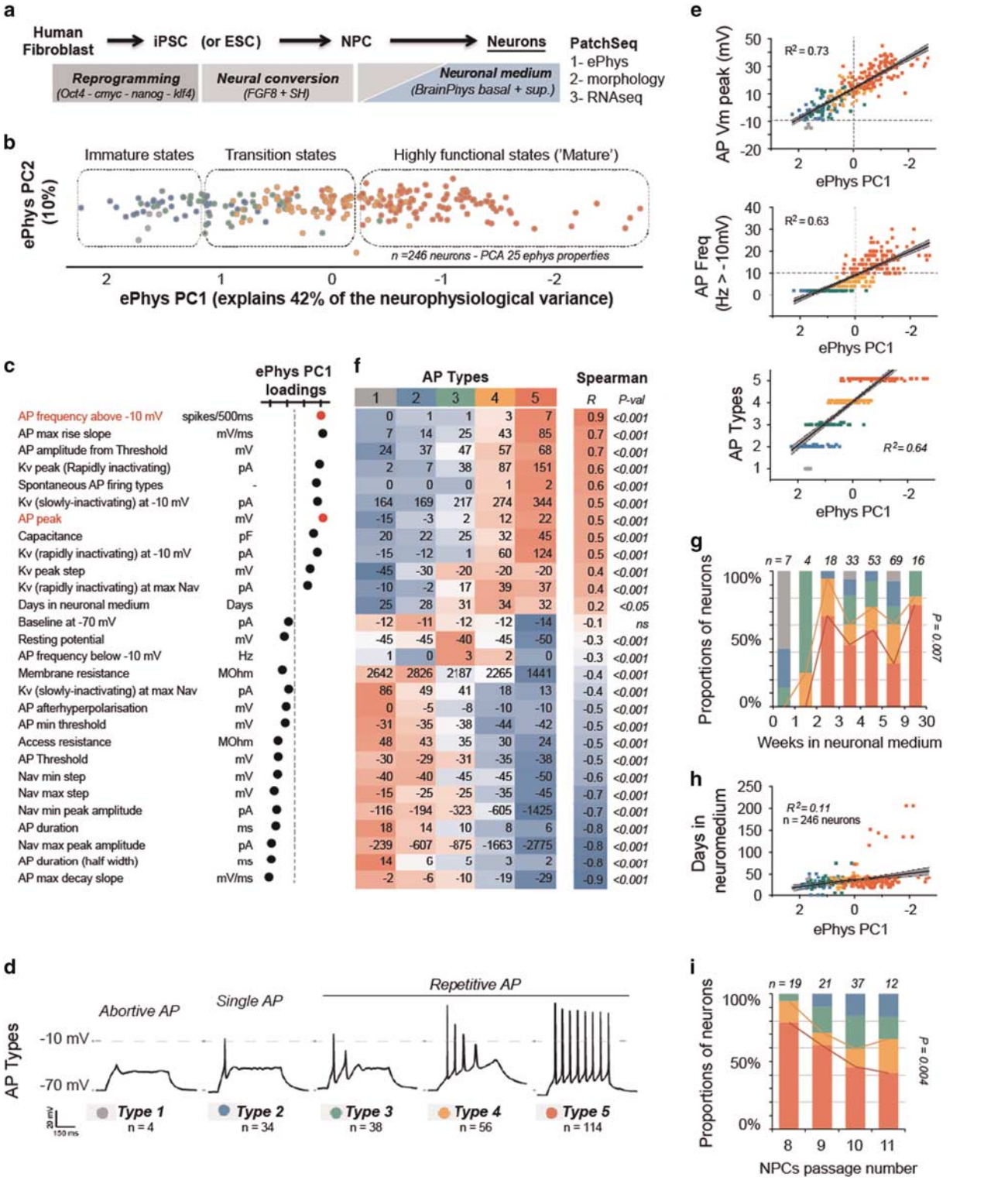

differentiated towards midbrain NPCs using an established protocol.[6] NPCs were expanded for 5–11 passages and re-plated in neuronal medium (BrainPhys basal+serum free supplements) that enabled differentiation and maturation under conditions supporting optimal electrophysiological activity.[13] Following this protocol, the human NPCs differentiated into cultures comprising about 50% astrocytes (GFAP+) and 50% neurons (TUJ1+/MAP2+). We did not use additional feeder layers of astrocytes for initial neuronal maturation. On the basis of immunostainings, we estimated that the neural circuits were formed with a majority of glutamatergic neurons (~62%) and smaller percentages of GABAergic neurons (~27%, GABA+) and dopaminergic neurons (~11%, TH +).[13] On the basis of patch-clamping data, we also found that neurons in highly functional states received 2.3 times more spontaneously active AMPA-mediated synaptic inputs than GABAergic synaptic inputs. The neurons were analyzed after ~30 days on average in neuronal medium (the full range tested throughout the entire study was 0–30 weeks). Each cell was tested with a consistent electrophysiological patch-clamping protocol measuring voltage-gated Na+/K+ currents, evoked and spontaneous APs, membrane resistance, resting potential, capacitance and synaptic activity (AMPA/GABA) (Supplementary Figure S1) and was filled with a dye (rhodamine) to allow morphological reconstruction. The same live cells were also collected for RNA-seq analysis.

Electrophysiological traits of human neurons *in vitro* reveal a continuum of functional states

We used unbiased statistical analyses to identify the broad range of functional states of differentiated neurons *in vitro*. To define the functional properties of each neuron, we performed a series of patch-clamping tests (Supplementary Figure S1). Then, we applied a PCA on 25 electrophysiological measurements mostly reflecting the functional intrinsic properties of 246 patch-clamped neurons (Figure 1b; ePhys PCA features and corresponding loadings listed in Figure 1c). Such analysis aimed to describe objectively the inherent variation in the basic electrophysiological profiles of human iPSC-derived neurons that is routinely observed *in vitro* by many independent laboratories. The first principal component, ePhys PC1, explained 42% of the variation in the dataset (Supplementary Figure S2A), and revealed a continuum of functional neuronal states that we separated into three broad groups: 'immature states,' 'transition states' and 'highly functional states.' These neuronal states appeared to reflect increasing stages of electrophysiological maturation. In support, we found significant correlations with several properties that are associated with neurophysiological development. The strongest correlation was obtained with AP firing properties. Indeed, the amplitude ('AP peak') and the firing rate ('AP frequency above −10 mV') of evoked APs stand out as two of the most influential loadings in PC1 (Figure 1c). We combined these two AP metrics to further categorize the neurons into five 'AP Types' (Figure 1d; Supplementary Figure S2B), which significantly aligned with ePhys PC1 (Figure 1e, $P < 0.01$). Our analysis suggests that either metrics —'ePhys PC1' or 'AP Types'—can be used objectively to determine the functional states of human neurons *in vitro*. Importantly, we demonstrated that these metrics largely reflect stages of neurophysiological maturation. For instance, we found significant correlations of AP Type classification with several other electrophysiological properties that typically associate with neuronal maturation, such as the cell membrane resistance, which is typically lower in more mature neurons (Figure 1f; Supplementary Figure S2D). Naturally, neurodevelopment also correlates with time spent in culture, and indeed we found a smaller fraction of AP Type 4 or 5 neurons in the first 3 weeks in neuronal medium than at later time points (Figure 1g). We also found a significant correlation of the PC1 variance with the time the cells spent in neuronal medium. However, the correlation between time in culture and the functional state of the neurons was rather weak

Figure 1. Human neurons in culture can be categorised into different electrophysiological states. (**a**) Human embryonic stem cells (ESCs) (H9) or human-induced pluripotent stem cells (iPSCs) from healthy subjects were converted to neuronal progenitor cells (NPCs). Neurons and astrocytes derived from the same progenitors were then cultured in neuronal medium (BrainPhys basal medium with supplements). See 'Materials and methods' section for more details. (**b**) Principal component analysis (PCA) of 25 electrophysiological properties (listed in **c**) measured with patch clamping of human neurons ($n = 246$). This PCA integrates basic cell-intrinsic electrophysiological properties such as passive membrane properties, voltage-dependent sodium and potassium currents and action potentials (APs) firing. Each dot represents a neuron. Astrocytes or any cells that did not express at least small voltage-dependent sodium currents were not included in the PCA. Cells that did not have unambiguous analysis of all the chosen 25 properties were also excluded from this PCA. (**c**) The dot graph represents the relative values of the loadings onto the first principal component (PC1) for each of the 25 properties used in the above PCA. The loadings highlighted in red correspond to the two measures that were used subsequently to define a continuum of five functional states. (**d**) Representation of the typical heterogeneous neuronal responses to optimal depolarizing current steps for 500 ms (Vm rest clamped around −70 mV). We classified those heterogeneous states of differentiated neurons into a continuum of five AP Types based on the combination of key electrophysiological properties identified with unbiased PCA: (1) the maximal peak of AP (Vm measured at the top of the best evoked AP), and (2) the frequencies of APs overshooting −10 mV. The same neuronal color key throughout the figure corresponds to this AP Types classification (Supplementary Figure S2B). (**e**) The graphs show the PC1 value for each neuron ($n = 246$) against the key AP properties and the corresponding AP Type classification. EPhys PC1 values highly correlate with the maximum peak and frequencies of APs (evoked APs freq were counted only if overshooting −10 mV in response to a square pulse of current of 500 ms from resting −70 mV). Linear regression fits ± 95% confidence intervals are shown. (**f**) Most measurements listed on each row significantly correlate with the AP Types classification (columns 1–5 of heat map). The values in the central heat map represent the median for the neurons in respective AP Type categories. To illustrate the direction of the measurement variations between AP Types, we color coded the heat map (values normalized by row with mean = 0 and variance = 1) from low to high values (blue, to white, to red). The last two columns show the Spearman's correlation coefficient (*R*) and its significance (*P*-val) between the measurements (row) vs the numerical class (1–5) of AP Types. The properties were sorted by decreasing correlation coefficient obtained. The *P*-values were corrected for multiple hypothesis testing (Bonferroni correction: $P < 0.05$ (2E-03), $P < 0.01$ (3E−04), $P < 0.001$ (3E−05)). (**g**) The differentiated neurons were patch clamped after different periods in neuronal medium. Days were counted from the switch of neuronal progenitor medium to neuronal medium (BrainPhys basal+supplements from 0 to up to 7 months). The proportion of more functional neurons (Type 4 and 5) significantly increased the first 3 weeks in neuronal medium, implying that an early maturation phase corresponds with the development of electrophysiological types; however, the proportions of Type 4 and 5 appeared to plateau after that period. The significance of this relationship in single neurons was measured with Spearman correlation between days in neuronal medium (*x* axis) and the numerical class (1–5) of AP Types. (**h**) We found a significant but poor correlation of the time spent in neuronal medium and functional states (measured by ePhys PC1 or AP Types). (**i**) After expansion (six passages) and storage at −80 °C, NPCs derived from the same cell line (H9) were thawed and cultured for another two to five passages before re-plating in neuronal medium. The neurons ($n = 89$) were patch clamped after 4–6 weeks in neuronal medium and categorized into AP Types. The proportion of Type 5 neurons significantly decreased with high NPC passage numbers. The significance of this relationship in single neurons was measured with the Spearman correlation between passage numbers (*x* axis) and the numerical class (1–5) of AP Types.

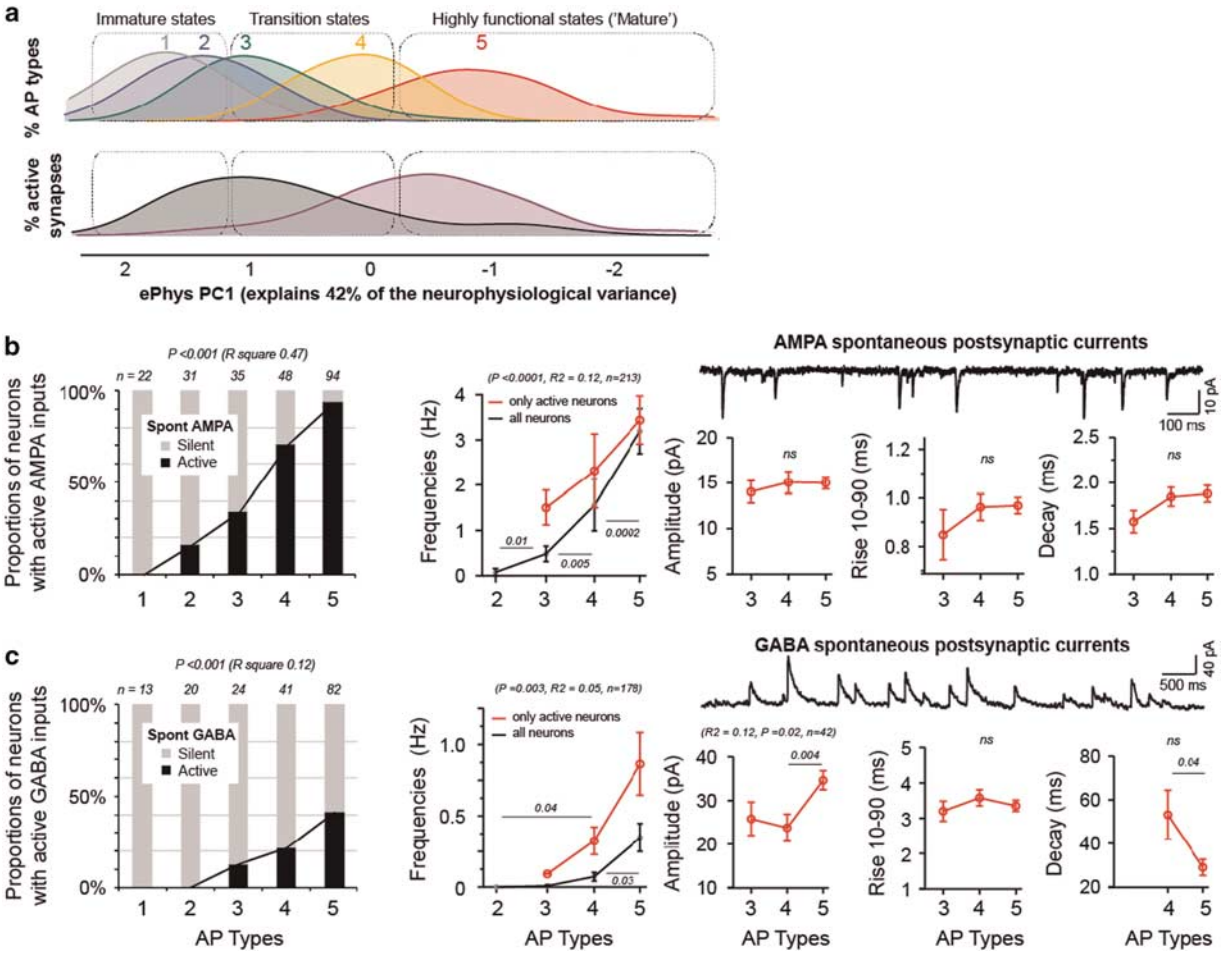

Figure 2. Synaptic input activity highly correlates with action potential (AP) states. (**a**) Frequency distribution of AP Types and differentiated neurons with active synaptic inputs against the ePhys PC1 measure in Figure 1b. (**b**) The trace represents typical spontaneous (Spont) AMPA events (NBQX-sensitive). Patched neurons were classified as synaptically active (active synaptic inputs) in the left histogram if more than three clear glutamatergic spontaneous events were detected (with typical AMPA kinetics and amplitude above noise levels) within 5-min recordings in voltage clamp close to the reversal potential of Cl^- channels (−70 mV). (**c**) The trace represents typical spontaneous GABA events (Gabazine-sensitive). Patched neurons were classified as pre-synaptically active in the left histogram if more than three clear GABAergic spontaneous events were detected (with typical GABA kinetics and amplitude above noise levels) within 5-min recordings in voltage clamp close to the reversal potential of Na^+ channels (0 mV). (**b**,**c**). Mean ± s.e.m. shown. For the spontaneous events amplitudes, the medians were 13% lower than mean but strongly correlated ($R^2 = 0.90$, $P < 0.0001$). For each graph a linear regression was fitted and the significant *P*-values were noted in brackets with R^2 and *n*. Non-significant regression fit *P*-values > 0.05 were noted as '(ns)'. Additional statistics between individual types were performed with the Mann–Whitney two-tailed test, and only the significant *P*-values from these tests were noted in the graphs above each compared group.

(Figure 1h), which may be a consequence of the fact that single human neurons differentiate at variable rate *in vitro*. In addition, different tissue culture practice may influence the efficiency and speed of maturation. For example, we found that simply increasing the passage number of NPCs before neuronal differentiation significantly reduced the proportion of Type 5 neurons within subsequent cultures (Figure 1i). Similarly, various cell lines may generate variable proportions of AP Type 5 neurons. We propose that, to identify accurate neuronal phenotypes between cell lines (for example, patients vs healthy subjects), it is important to compare neurons of equivalent functional states, rather than relying exclusively on the time the cells have spent maturing *in vitro*.

Synaptic activity correlates with AP Types

Synaptic activity is the essence of neuronal communication and its disruption is often the cause of behavioral defects in neurological disorders. Therefore, many recent studies have focused on measuring possible synaptic abnormalities in IPSC-derived neurons in the modeling of neural diseases *in vitro*.[23–26] As synaptic activity is associated with the functional maturity of neuronal circuits,[27] we examined the relationship between spontaneous synaptic activity and our AP-Type categories (Figure 2a). Our culture protocol generated roughly two times more glutamatergic neurons than GABAergic neurons. This bias was strongly reflected in a higher likelihood to record spontaneous active excitatory inputs than GABAergic synaptic inputs. Despite those differences, we found that both AMPA and GABA activity significantly increased along the continuum of AP Types (Figures 2b and c). In our conditions, 95% of AP Type 5 neurons received active pre-synaptic inputs, whereas only ~10% of Type 2 neurons did. This result is particularly important to consider in iPSC disease models, which compare synaptic functions between patients. Overall, our analysis highlights the point that, if neural cell lines do not have similar proportions of AP Types, such variability will influence differences in the measured synaptic activity.

Neuromorphological features of AP Types

To further investigate how our classification of AP Types reflects neurodevelopmental stages, we filled 256 patched neurons with

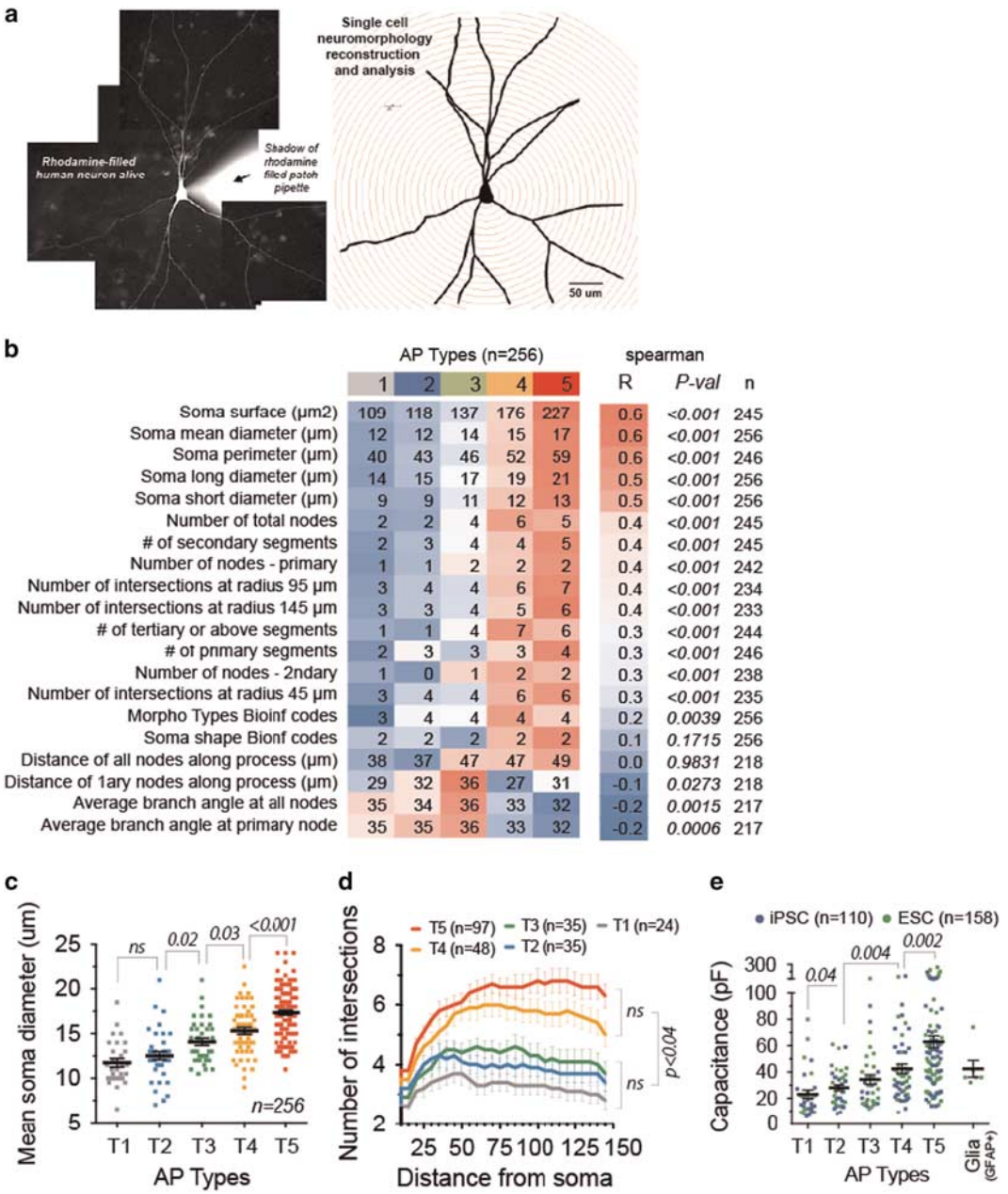

Figure 3. Morphological features that correlate with action potential (AP) states. (**a**) Stitched photos of a live patched neuron, which was filled with rhodamine (left) and morphogically reconstructed with neurolucida (right). (**b**) Correlation of morphological measurements (rows) with AP Types (columns 1–5). The values in the central heat map represent the median for the neurons in respective AP Type categories. To illustrate the direction of the measurement variations between AP Types, we color coded the heat map (values normalized by row with mean = 0 and variance = 1) from low to high values (blue, to white, to red). The last two columns show the Spearman correlation coefficient (*R*) and significance (*P*-val) of the Spearman's rank correlation between the electrophysiological measures (row) and the numerical class (1–5) of ePhys Type. The properties were sorted by decreasing correlation coefficient. (**c**) Mean soma diameter significantly increased in more functional AP Types. (**d**) Sholl analysis revealed that more functional AP Types had significantly more complex dendritic/axonal arborization. Mann–Whitney *U* two-tailed tests were performed at 20, 50 and 100 µm between different types. The dendritic complexities of Type 4 and 5 neurons were not significantly different, and the complexity between Types 1, 2, 3 was not either. However, Types 4 and 5 were significantly more complex than Types 1, 2, 3. Mean ± s.e.m. shown. (**e**) The capacitance significantly increased in more functional AP Types of neurons. Significance threshold was $P < 0.05$. Mann–Whitney *U* two-tailed *P*-values are shown in **d**, **e**.

an inert red dye (rhodamine) and reconstructed their morphology (Figure 3a). We analyzed 20 morphological features (listed in Figure 3b; Supplementary Figure S3C) and found that the size of the soma and the complexity of neurite arborization increased in higher AP Types (Figures 3c and d). The arborizations of Type 4 and 5 neurons were significantly more complex than those of Types 1, 2 or 3. Furthermore, the increase in soma size and distant arborization complexity were consistent with larger intracellular volume, which was estimated with the cell capacitance. Despite high cell-to-cell variabilities even within functional states, the most highly functional neurons (i.e., AP Type 5) tended to have overall significantly larger intracellular volume (Figure 3e). This

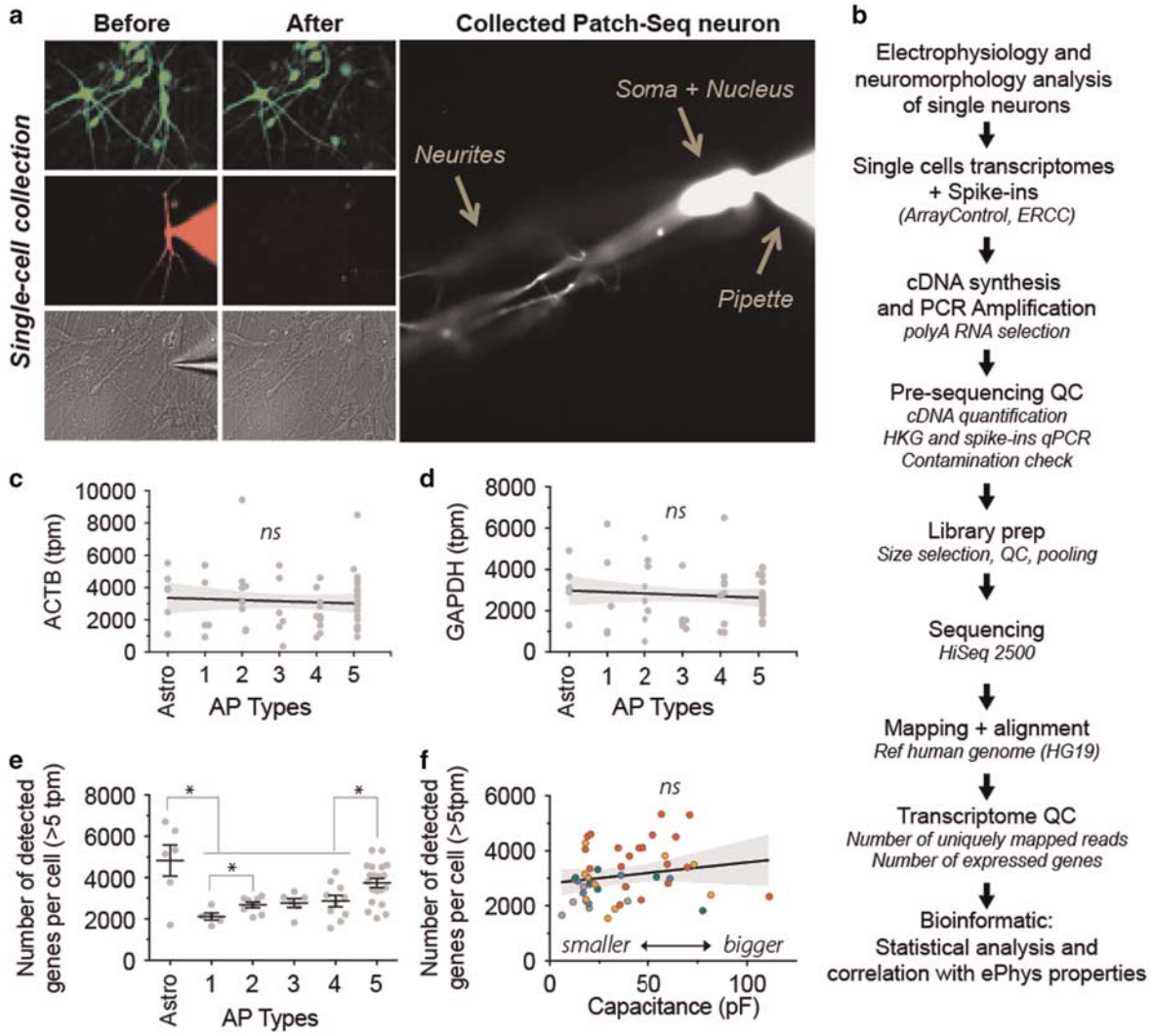

Figure 4. Whole-single-cell RNA-seq of patch-clamped neurons (PatchSeq). (**a**) The photos show an example of neuronal culture stained with eGFP before and after a single neuron was patched and collected for transcriptome analysis. For every cell included in the analysis, the entire neuron was collected, including the soma/nucleus and neurites. The photos permitted us to confirm that only the patched neuron filled with rhodamine was collected, leaving the surrounding tissue intact. (**b**) Following electrophysiological and morphological analyses of live neurons, the single cells were collected and their transcriptome processed for deep sequencing, bioinformatics processing and statistical analysis. (**c**,**d**) Housekeeping genes such as ACTB and GAPDH were detected in every cell. Their expression levels were not significantly different between types of neurons and astrocytes. (**e**) Significantly more genes were expressed in astrocytes and Type 5 neurons compared with the other neuronal types. Asterisks represent Mann–Whitney *P*-values < 0.05. (**f**) The number of detected genes above 5 tpm did not significantly correlate with the size of the neurons, estimated here by capacitance. The action potential (AP) Types are color coded in the graph (red T5, orange T4, green T3, blue T2, gray T1).

Figure 5. Single-cell transcriptomes segregate functional states of differentiated neurons. Unbiased and unsupervised analysis was performed on the transcriptome (17 757 genes detected > 5 tpm in at least one cell) on a sample of 56 whole single-cells (including nucleus, soma and distant neurites), which passed all QC. This sample comprised 50 differentiated neurons displaying Nav currents and six astrocytes expressing GFAP:eGFP. (**a**) Unsupervised clustered heat map of cell-to-cell transcriptome correlations (Euclidean distances). The linkage distances of the hierarchical clustering represent an estimate of the quality of the unbiased/unsupervised clusters. (**b**) Unsupervised principal component analysis on the entire single-cell transcriptomes. Cell transcriptome profiles (symbols) are represented in a two-dimensional principal component space. These unsupervised analyses reveal molecular segregation between groups of neurons in highly functional states (almost all action potential (AP) Type 5–85%), less functional neurons in 'transition states' (mix of different AP Types with significantly less Type 5–15%) and astrocytes. Furthermore, the functional molecular clusters surpassed transcriptional differences between iPSC lines from different subjects and even an embryonic stem cell line. (**c**) Monocle analysis illustrates the progress through functional states by pseudotemporal ordering of single-cell mRNA expression profiles. Cell expression profiles (points) are represented in a two-dimensional independent component space. Lines connecting points represent edges of the minimum spanning tree constructed by monocle. Solid black line indicates the main diameter path of the minimum spanning tree and provides the backbone of monocle's pseudotime ordering of the cells based on molecular profiles. (**d**) The expression of five key neurotransmitter genes in 20 sequenced Type 5 neurons was normalized and compared to determine their neurotransmitter identity. Most cells could be classified as either glutamatergic, GABAergic, dopaminergic, or serotonergic and a few cells remained undefined. (**e**) Heat map of single-cell gene expression levels. The genes were selected and grouped based on known neuronal functions. For comparison, AP Type 5 genes identified in the present study are in red/bold (Supplementary Figure S5B). (**f**) Genes significantly correlating with numerical AP Types classification by the Spearman's rank correlation coefficient ($P < 0.001$).

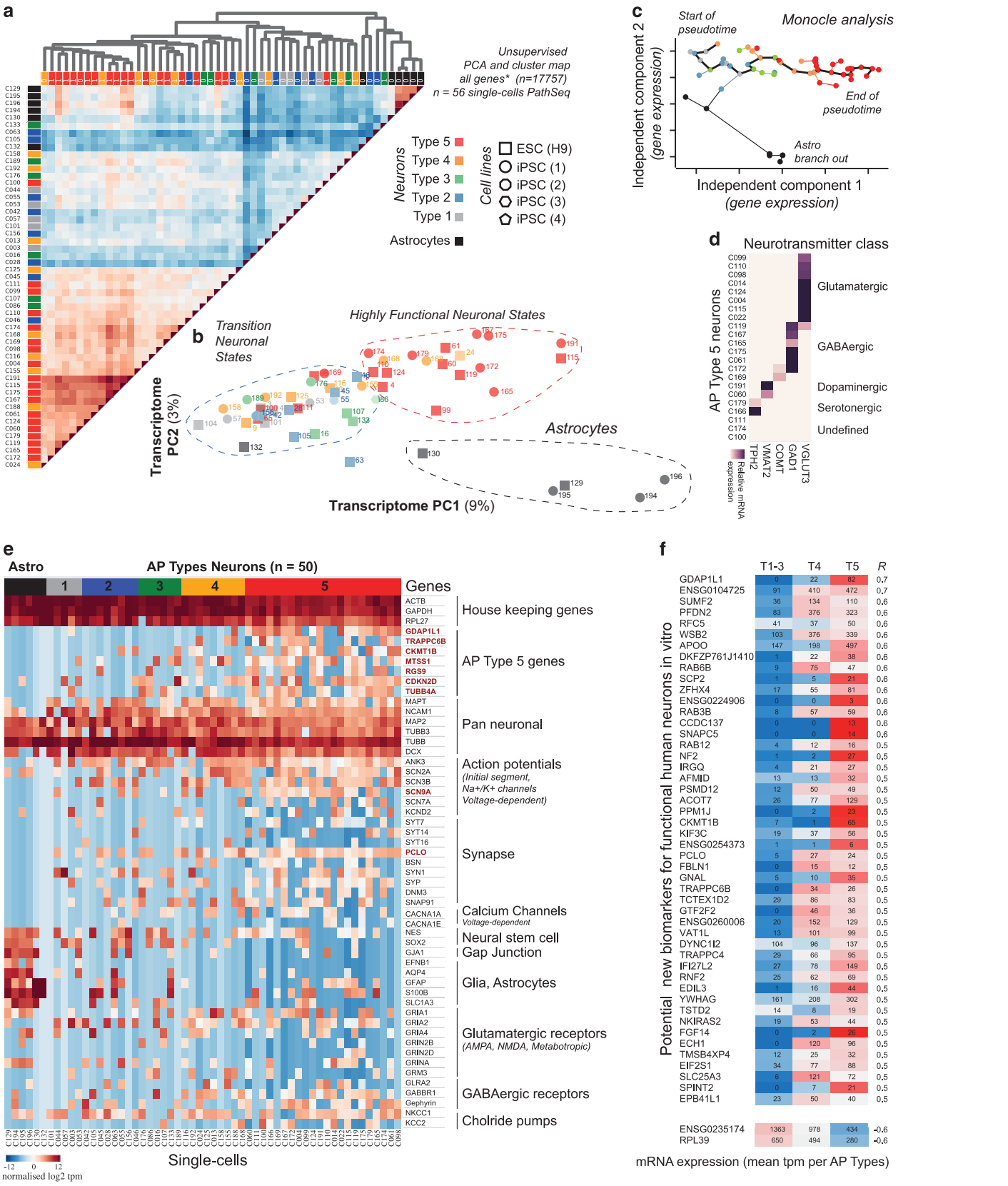

multimodal analysis demonstrates that the electrophysiological states correlate with morphological neurodevelopmental phenotypes.

Single-cell transcriptome analysis of patch-clamped neurons

To examine the relationship between gene expression and electrophysiology, we generated single-cell transcriptome data from the same neurons that were analyzed for electrophysiology and morphology. At the end of the patch clamping and imaging protocol, which lasted about 30 min, each cell was isolated with negative pressure applied to the same pipette that was used for the whole-cell recordings. Images acquired before and after single-cell collection confirmed that only the targeted single cells were taken out, leaving surrounding cells in place (Figure 4a). Importantly, we collected the entire neuron, including the soma, nucleus and neurites (Figure 4a, right panel). Poly-A selected mRNA molecules were reverse transcribed to cDNA and amplified immediately after patching and isolation to avoid RNA degradation. Before RNA-seq library preparation, we subjected the cDNA from each cell to a set of QC criteria to exclude potentially low-quality captures and amplifications (Figure 4b). We then generated RNA-seq libraries from amplified cDNA. Highly expressed housekeeping genes such as ACTB and GAPDH were readily measured, and quantitative real-time PCR measurements significantly correlated with sequencing read counts (Figures 4c and d; Supplementary Figures S4A and B). The transcript abundances of artificial RNA spike-ins mixed in with the single-cell RNA (ERCCs and ArrayControl spike-in RNA standards) were also highly correlated with the normalized sequencing counts (FPKM) (Supplementary Figure S4C). These observations support the quality of our single-cell transcriptomics data. To minimize erroneous conclusions that arise from lowly expressed, highly varying genes, we excluded reads that were detected below 1 tpm. In addition, a small number of cells ($n = 3$) with fewer than 2000 genes detected above 5 tpm were excluded. Without these outliers, an average of ~3000 genes per cell was detected above >5 tpm (Figure 4e). Interestingly, the number of genes detected was significantly higher in Type 5 neurons and astrocytes than in less active AP Types (Figure 4e). However, we found no significant correlation between the number of detected genes (>5 tpm) and the size of the cells (Figure 4f).

Molecular signatures distinguish neuronal functional states *in vitro*

To examine variation in the single-cell gene expression, we excluded the outliers with trace of DNA contamination, abnormal expression level of housekeeping genes, damaged axons and dendrites from the collection, unstable physiological recordings before collection, abnormal cDNA quantity, low number of uniquely mapped reads and low number of detected genes. We then performed a hierarchical clustering analysis and PCA with the transcriptomes of 56 single cells (50 differentiated neurons, and 6 astrocytes) that passed all QC (Figures 5a and b). This unsupervised and unbiased single-cell RNA-seq analysis revealed a distinct transcriptome cluster of neurons corresponding to highly functional states (83% AP Type 5 neurons—17% AP Type 4 neurons). This highly functional cluster separated from astrocytes and a mixed group of neurons that represents 'transitory' neuronal states (Figure 5b; Supplementary Figure S5A). Furthermore, the molecular profiles of cells in distinct functional states grouped together, independently of individual genetic background (cell lines from different subjects) and the time spent in culture (Figures 5a and b).

To better recapitulate the transcriptional dynamics of functional states, we also demonstrated the molecular trajectory of the electrophysiological maturation by applying monocle analysis.[28] Interestingly, AP Types 1 and 2 clustered at the beginning of the pseudotime and branched out towards astrocytes (GFAP+) or towards AP Type 3 and 4 neurons, and highly functional AP Type 5 neurons clustered at the end of the pseudotime (Figure 5c). Together, these results indicate that mRNA expression correlates strongly with neurophysiological states.

To obtain physiologically relevant neuronal circuits, we generated mixed cultures of neurotransmitter classes and astrocytes. The patch clamping was not targeting a specific subpopulation of neurons, and most patched cells were tagged with Synapsin:eGFP lentivector. Therefore, to better characterize our sample, we isolated the AP Type 5 neurons that were sequenced ($n = 22$) and determined the nature of their neurotransmitter classes. On the basis of the normalized expression of five known genes, most Type 5 neurons segregated into different neurotransmitter classes (36% glutamatergic VGLUT3, 27% GABAergic GAD1, 14% dopaminergic VMAT2 or COMT, 9% serotonergic TPH2 and 14% undefined neurons) (Figure 5d). These results demonstrate that our functional classification is sufficiently broad to incorporate more detailed subcategories of various neurotransmitter classes.

To further characterize the molecular profiles of differentiated neurons in various functional states, we compared the single-cell mRNA expression of 45 genes typically known for their importance to neuronal functions (Figure 5e; Supplementary Figure S5B). Not surprisingly, most well-known neuronal genes (for example, pan neuronal, synaptic, APs, ion channels genes) were expressed in all the differentiated neurons in our sample. Typical astrocytic/glial genes (for example, AQP4, GFAP, S100B, GJA1, SLC1A3, EFNB1) were expressed in astrocytes, which were identified based on LV marker GFAP:tdTomato, distinctive morphology and electrophysiology. Genes typical of early neuronal development (for example, SOX2, NES) were expressed mostly in immature AP Types and some astrocytes. A few neuronal genes appeared expressed in all AP Types and even in astrocytes/glia (for example, MAP2, TUBB3, TUBB). Interestingly though, many neuronal genes that were exclusive to neurons expressed at similar levels in all AP Types (for example, MAPT, NCAM1, ANK3, SYN1, SYP). Therefore, we asked whether some genes may specifically express in highly functional AP Types of neurons. We first assessed the Spearman's correlation between gene expression and AP Type classification, which revealed 45 genes that most significantly correlated (Figure 5f). Some of these genes have known neuronal functions such as synaptic plasticity (for example, RAB3B,[29,30] PCLO/Piccolo) or voltage-gated sodium channels (for example, SCN9A/Nav1.7). However, interestingly, a majority of these genes have not been investigated before for specific neuronal functions and may be used as new potential biomarkers to identify functional human neurons *in vitro*. This finding then led us to propose that single-cell gene expression data has utility in the prediction of the electrophysiology of human neurons.

Machine-learning classifiers integrate transcriptome features to predict functional states

To identify the single-cell transcriptomics signature important to predict functional states, we trained an Extremely Randomized Trees classifier using 56 single cells (Figure 6a). We used a randomized 10-fold cross-validation to evaluate the performance of the algorithm in classifying cells in different functional state categories (Figure 6). In Figure 6, we illustrated the results of three classifiers: the first one isolates AP Types 4–5 neurons with 92% accuracy in a mixed population including astrocytes (Figure 6b); the second isolates AP Type 5 neurons with 83% accuracy in a population of differentiated neurons only (Figure 6c); and the third isolates highly functional neuronal states (based on transcriptome PCA clustering in Figure 5b) with 86% accuracy in a population of differentiated neurons only (Figure 6d; Supplementary Figure S6A). For higher accuracy (more true positive), the classifiers can be trained differently by adjusting the 'classifier

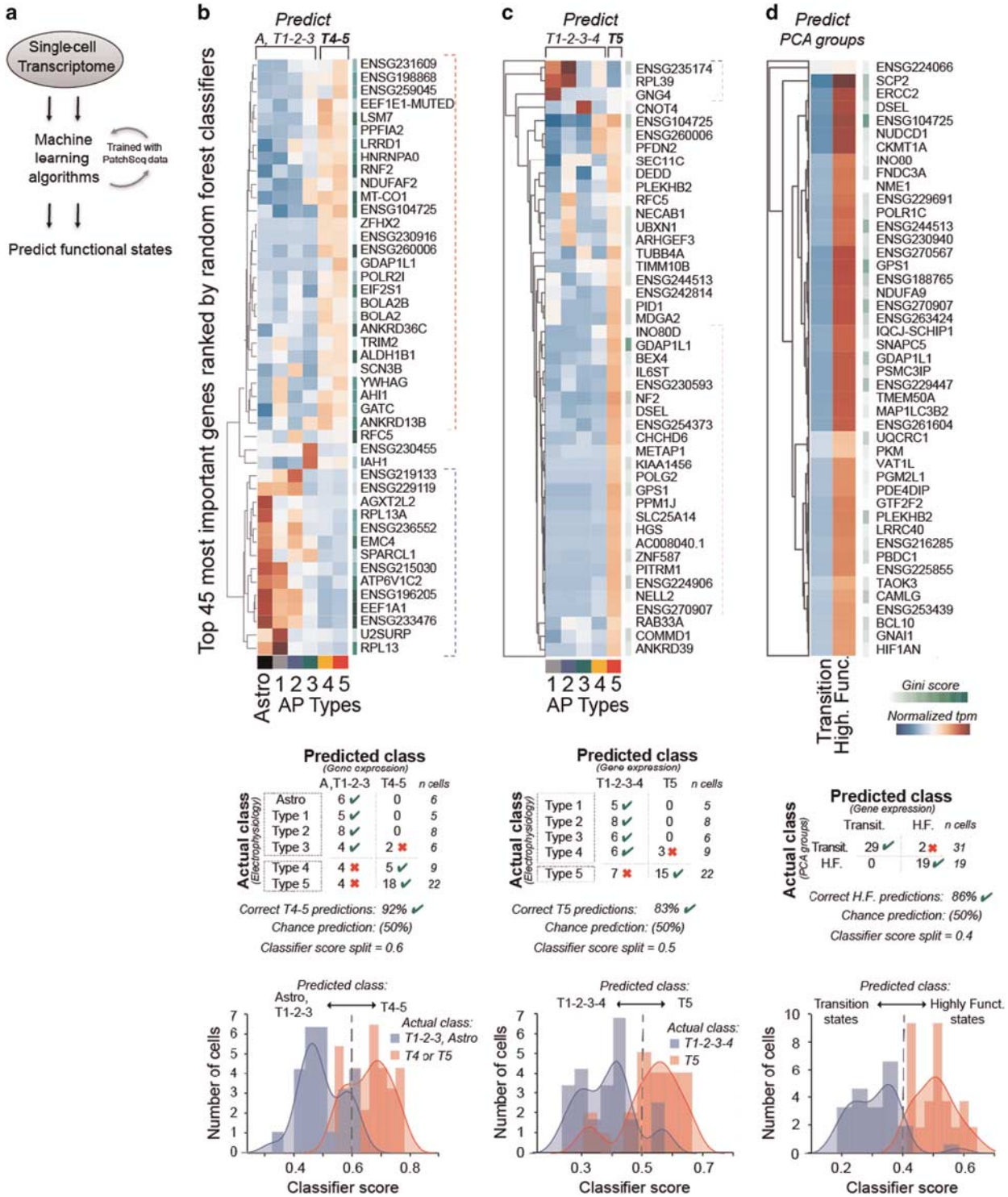

Figure 6. Machine-learning tree classifiers predict functional states of neurons based on single-cell transcriptome and reveal potential biomarkers. (**a**) Extremely randomized trees (ERT) classifier built with the transcriptome of 56 single cells and trained with electrophysiological data. Actual classes were attributed by electrophysiological measurements. Predicted classes were attributed by the machine-learning algorithm based on single-cell transcriptomes. (**b–d**) Each ERT classifier was trained to categorize the cells in two functional classes. Classifier B was trained to predict AP Types 4–5 in a mixed group of cells including differentiated neurons and astrocytes. Classifier C was trained to predict Type 5 neurons from other differentiated neurons. Classifier D was trained to predict highly functional (HF) neurons from other differentiated neurons in transitional states determined by the principal component analysis (PCA) clusters. The lists show the top 45 genes selected by the ERT classifier with the highest Gini scores. The green heat map columns represent the normalized importance of each gene attributed by the classifier (Gini score). The blue-red heat map matrices represent the mean expression normalized (mean 0 and variance 1) of each gene from high (red) to low (blue) in actual cell types. The genes were ordered by Euclidean clustering of the gene expression by actual functional states. Confusion matrices are displayed below the heatmaps. The confusion matrices values represent the numbers of cells in each category. Predictions were annotated with a green checkmark if correct and a red cross if false. The test-fold score for each cell was recorded and a score histogram was computed for each cell group (blue and red bars). Classes were predicted with a determined classifier score split, indicated by a gray dashed line in the histograms. See also Supplementary Figure S6.

score split,' but the algorithm may also generate more false negatives, resulting in lower sensitivity. The area under the curve of the receiver-operating characteristic, which is a measure of the trade-off between sensitivity and specificity, was 0.93, clearly above random prediction (0.50) (Supplementary Figure S6B). The unbiased training algorithms selected and weighted the optimal genes to predict functional types (Figure 6).

Identification and isolation of functional neurons with a GDAP1L1 promoter-driven eGFP viral vector

In addition to the machine-learning classifier, we performed an in-depth differential expression analysis to reveal a complementary set of genes specifically expressed in Type 5 neurons (Figure 7a). Altogether, we performed three independent unbiased analyses to identify a total of 165 genes (Supplementary Table S1) related to specific electrophysiological functional states (Spearman correlation in Figure 5f; machine-learning in Figures 6b–d, differential expression in Figure 7a). Among the most highly ranked genes, 29 genes appeared in more than one analysis (Supplementary Table S1). Only one gene appeared in all of those independent analyses—GDAP1L1. GDAP1L1, which is the human paralog of the ganglioside GDAP1, had been previously suspected to have an important function in neuronal cells because of its high abundance in brain tissues.[31] Interestingly, GDAP1L1 mRNA is expressed exclusively in brain tissues in human (Supplementary Figure S7A). We confirmed with immunostaining that GDAP1L1 protein was present in human iPSC-derived neurons but not in astrocytes (Figure 7b). Our immunohistochemistry staining also suggested that GDAP1L1 was only present in a subset of TUJ1+ neurons (Figure 7c), presumably highly functional neurons

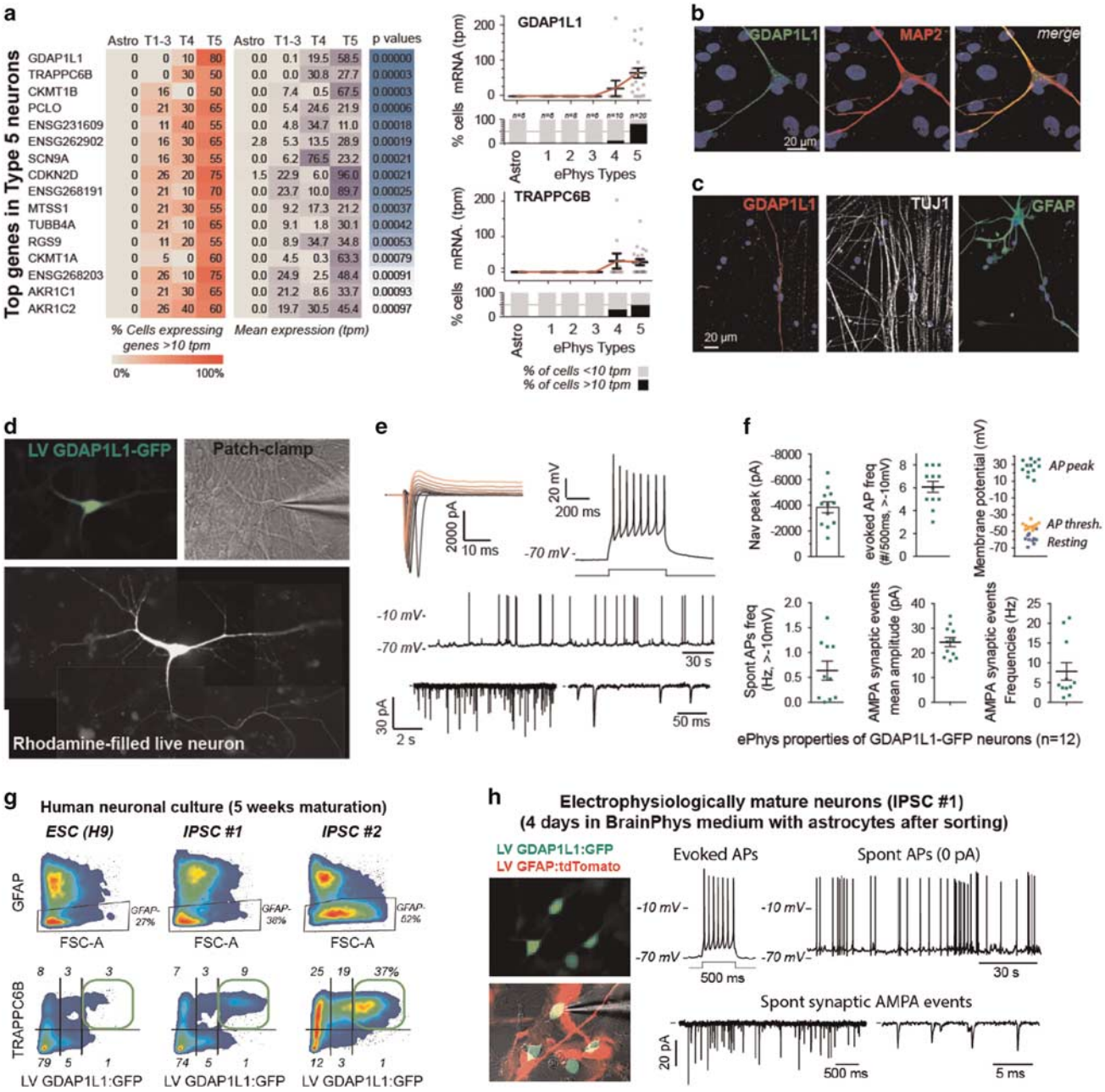

(Type 5). To confirm this hypothesis, we constructed a LV expressing GFP under the control of the GDAP1L1 promoter. We infected three different cell lines of human neurons with the vector (Figure 7d, see also Supplementary Figure S6 for additional immuno-histochemistry of vector). Although GDAP1L1 mRNA and protein were not found in astrocytes, the eGFP under the control of GDAP1L1 gene promoter was occasionally found in astrocytes (GFAP+). Nevertheless, we patched the neurons with the brightest eGFP and clear neuronal morphology and found that all of them were highly functional neurons ($n = 10/12$ were Type 5, $n = 2/12$ were Type 4, and $n = 11/12$ neurons had clear spontaneous AMPA synaptic activity) (Figures 7e and f). Next, we asked whether this strategy could be used to isolate mature functional human neurons by a higher-throughput technique. With that aim, we derived NPCs from three different cell lines and differentiated them into neurons for ~4 weeks in neuronal maturation medium. Then, we infected the neuronal cultures with two LV, GDAP1L1-eGFP (to identify functional neurons) and GFAP-tdTomato (to identify astrocytes). A few days later we processed the cells with FACS. After exclusion of dead cells and GFAP+ cells, we isolated a population of neurons with high GDAP1L1-eGFP expression (Figure 7a). This subset of neurons with high GADAP1L1-eGFP also showed particularly high abundance of TRAPPC6B protein (measured with primary antibody) (Figure 7a). TRAPPC6B is another top gene candidate that appeared from our transcriptome analysis to be predictive of highly functional neurons. This finding further supported our premise that this subpopulation of high GDAP1L1-eGFP neurons represents the electrophysiologically active states. Therefore, we repeated the FACs experiment with live cells differentiated for ~4 weeks and sorted out three subsets of live cells: (1) presumably highly functional neurons (GDAP1L1:eGFP-highly positive and GFAP: tdTomato-negative), (2) astrocytes (GFAP:tdTomato-positive and GDAP1L1:eGFP-negative) and (3) the rest of the cells, including less functional neurons (Supplementary Figure S8). We then re-plated 50 000 neurons with high GDAP1L1-eGFP per well (48-well plate) onto a glass coverslip coated with a layer of human cerebellum astrocytes. Four days after re-plating, we patch-clamped the GDAP1L1:eGFP-positive sorted cells and confirmed that they were highly functional Type 5 neurons (Figure 7b, $n = 5/5$). Altogether, we believe these findings demonstrate a first proof of concept that the genes identified in our multimodal analysis may be used as biomarkers to help identify, enrich or isolate highly functional states of iPSC-derived human neurons *in vitro*.

DISCUSSION

Studies of post-mortem human brain tissues have revealed some molecular and anatomical features in neurodevelopment and in the adult brain.[32] However, studying the neurophysiological properties of live single neurons in the human brain is technically challenging and so far has been mostly restricted to animal models, occasionally to brain slices of aborted human fetus,[33,34] and more recently to human neuron cultures reprogrammed from fibroblasts.[13,16,25,26,35,36] In this study, we have bridged human neurophysiology and gene expression by integrating single-cell electrophysiology, morphology and transcriptomics analysis of live human neural cells.

Single-cell PatchSeq: multimodal analysis of electrophysiology, morphology and transcriptomics profiles

Recent breakthroughs in single-cell transcriptomics methods have emphasized the importance of identifying different biological types of cells.[37–47] To resolve the diversity of cellular states, the use of single-cell analysis yields important insights that are masked or misrepresented in bulk RNA preparation from mixed cell populations.[39,48,49] For many years, only a few studies succeeded in applying gene expression analysis to patch-clamped neurons.[50–56] Here, we demonstrate the possibility of performing whole-transcriptome analysis on patch-clamped single human neurons derived from iPSCs or ESCs. Interestingly, many neuronal mRNAs are transported to the synapses and spines for rapid on-demand local translation.[57,58] Unlike most single-cell methods relying on tissue dissociation and flow cytometry, the method developed in this study processes the entire neuron and therefore includes mRNA from the nucleus, the soma and distant axons/dendrites, which may provide a more accurate representation of the transcriptome.[58] This approach may also be relevant for specific neurological disorders that may affect mRNA dendritic/axonal trafficking or the function of mRNA at synaptic sites.[59,60] Most importantly, in addition to the transcriptome profile, our method provides unique physiological and morphological information about the cells. Our results reveal the strong correlation

Figure 7. Biomarkers to isolate highly functional Type 5 neurons. (**a**) The top 16 genes expressed mostly in Type 5 neurons. The genes were selected based on the combination of several criteria: OFF (< 10 tpm) in all astrocytes, OFF in $> 70\%$ of Types 1-2-3 neurons, OFF in $> 50\%$ of Type 4 neurons, ON (> 10 tpm) in $> 50\%$ Type 5 neurons and then by the genes significantly more expressed in Type 5 vs all other cell types (*P*-values from a Mann–Whitney test). The selected genes were then ordered by *P*-values and the most significant 16 genes are shown ($P < 0.001$). Significance was tested with two-tailed Mann–Whitney *U* test between Type 5 neurons and all the other cells. The expression of the top two genes was plotted. Each gray point represents a single neuron. The red curve is the mean ± s.e.m. In the bottom charts black bars represent the proportion of cells in each cell type group with ON expression (> 10 tpm). (**b**,**c**) Immunostainings of fixed human neuronal cultures confirm the translation of GDAP1L1 at the protein level in some neurons (MAP2+, TUJ1+) but not in astrocytes (GFAP+). (**d**) Example of a live human neuron expressing eGFP under GDAP1L1 promoter and filled with rhodamine with the patch-clamping pipette. (**e**) Whole-cell patch-clamp recordings from GDAP1L1-eGFP neurons. The brightest GFP cells with neuronal morphology were selected for patch clamping after ~4 weeks in BrainPhys neuronal medium. The neurons expressed strong Nav/Kv currents (top left). The evoked APs were measured by slightly hyperpolarizing the cells to reduce spontaneous activity (top right). Spontaneous APs were recorded at resting membrane potential with zero current injected (middle). Spontaneous AMPA-mediated excitatory synaptic activity was recorded in voltage clamp at −70 mV (bottom). (**f**) The electrophysiological properties of the patched GDAP1L1-eGFP neurons ($n = 12$) were mature and functional. Means ± s.e.m. shown. The properties of single neurons are represented by each dot in the graphs. APs were counted only if amplitude was above −10 mV. Spontaneous AP frequencies were measured at resting membrane potential. (**g**) Three human neuronal cell lines, which matured for 5 weeks in BrainPhys basal+supplements, were infected with LV GDAP1L1:EGFP for 5 days before being dissociated, fixed and stained. Healthy cells not expressing GFAP (GFAP-neg; top graphs) were analyzed for their expression of TRAPPC6B protein and LV GDAP1L1:GFP expression (bottom graphs). The green rectangles highlight the cells expressing high levels of GFP under GDAP1L1 promoter and high levels of TRAPPC6B protein. The proportion of presumably mature ePhys types of neurons varied highly between the three cell lines. (**h**) Using two lentiviral vectors we sorted live astrocytes and live neurons from IPSC#1 after 5 weeks in BrainPhys and re-plated them on glass coverslips for 4 days before electrophysiological evaluation. The population of neurons expressing high levels of GFP under GDAP1L1 promoter (and no GFAP: tdTomato) were patched and all the cells were classified as highly functional neurons ($n = 5$) with on average high evoked firing frequencies (16 ± 2 Hz), low-resting potentials (−58 ± 2 mV), and large AP amplitude (91 ± 4 mV).

between functional and molecular profiles, validate the biological relevance of our methods merging patch-clamping analysis and single-cell RNA-seq, and demonstrate that transcriptome analysis can be used to predict the physiology of a cell. This approach can be applied to any kind of electrophysiological type of cell and may help to better define the cellular diversity in the brain.[61–64] Beyond the usefulness of such multimodal analysis in cellular neuroscience, this framework may also branch out to other fields of cell biology to correlate human cell physiology and molecular signatures.

Functional neuronal states and neurodevelopmental timeline *in vitro*

Typically, neurodevelopmental processes are described over a specific timeline. For example, newly born mouse neurons mature in pre-existing adult brain circuits by following a timed sequence of physiological events.[65,66] However, at the single-cell level, intrinsic and extrinsic programs can dynamically influence the rate and speed at which different human neurons reach functional states *in vitro*. The prediction of this maturation process is sometimes challenging as it may vary between cell types, individuals and species.[15–17] For example, the human brain matures over a longer period of time than most other species studied in laboratories. Similarly, human neurons *in vitro* usually take a longer time than rodent neurons to reach the equivalent maturity.[35] In addition, the technical variability of tissue culture protocols between independent labs makes 'time *in vitro*' an unreliable metric to objectively assess the functional maturity of neurons. As an alternative, we propose a method to efficiently quantify and isolate defined neurophysiological profiles *in vitro* based on data-driven features that do not require the measure of time *in vitro*. In this classification, we define the AP Type 5 neurons as a highly functional state of maturity; we define this stage as a broad minimal requirement to study functional human neurons *in vitro*. However, it is important to note that this stage is not necessarily terminal. For example, we have recorded the electrophysiological properties of neurons that were matured and kept in BrainPhys with supplements for more than 20 weeks and, whereas the broad properties used to define Type 5 neurons were indistinguishable from those of neurons maturing in the same medium for 6 weeks, we found that the membrane resistance significantly decreased over the longer time periods (for example, Type 5 neurons Rm was 1612+208 MOhm after 45 days in BrainPhys ($n = 17$) and 224+26 MOhm after 150 days in BrainPhys ($n = 11$), see also ref. 35). Furthermore, we based our functional state classification on a PCA that only integrated cell-intrinsic electrophysiological properties (25 features). Following this reasoning, we excluded synaptic input properties from that PCA because they most strongly depend on extrinsic neuronal network properties. This approach also allows us to use our classification model to compare synaptic function in cells of equivalent AP Types with less bias. Nevertheless, adding healthy synaptic activity to the PCA expands mostly PC2 and does not affect PC1 or our functional state classification.

Neuronal diversity

In the present study, we present an unbiased profiling of the electrophysiological states of human neurons *in vitro*. The framework that we propose here is sufficiently broad to include a wide heterogeneity of neuronal neurotransmitter classes (for example, glutamatergic, gabaergic, dopaminergic, serotonergic, motor neurons). Similarly, we found that each of our defined AP Types could be obtained from neurons categorized in various morphological classes (for example, bipolar, fusiform, pyramidal, multipolar; see Supplementary Figures S3A and B). Finally, the framework is also sufficiently broad to avoid masking relevant differences in disease modeling studies. The present study points out the importance of resolving broad neurophysiological states *in vitro*. Several other important studies have also highlighted the unique nature of cellular and brain region identities of neurons in rodents[55,56,62,63,67–70] and human brain.[71,72] The complex, precise, heterogeneous and dynamic assembly of 100 billion cells in the human brain is the best living illustration of cellular diversity in functional tissues. Interestingly, each neuron has the potential to be unique even at the genomic level.[73] The depth of the classification one should reach remains arbitrary.[62] Further work will be needed to deepen our broad functional states classification to more precise sub-classification. For example, it is possible that within AP Type 5 neuron categories, different neurotransmitter classes have subtle different physiological properties that they may acquire over various period *in vitro*. Regardless, our results point out the importance of stratifying neurons into equivalent functional states before investigating the differences among patients in disease models *in vitro*.

Models of neurological disorders *in vitro* will benefit from better characterization and quantification of electrophysiologically active human neurons

Advances in human cellular reprogramming have propelled a new wave of *in vitro* experiments to identify differences between healthy subjects and patients with neurological and psychiatric diseases.[24,74–77]

Studies of iPSC models *in vitro* have found that neurons obtained from patients affected by autism have significantly smaller soma, reduced dendritic complexity and less synaptic activity.[78] We found the same set of phenotypes when comparing less functional AP Types (Types 1-2-3) with more functional AP Types (Types 4–5). Together, these findings support the hypothesis that autistic neurons suffer from a general lack of functional maturity, which may cause an indirect defect in synapses. Being able to examine many cellular phenotypes simultaneously in the same single neurons may help to discern the causes of a disease from subsequent pathophysiological cascades and may be critical to the discovery of effective treatments.

Despite the huge promises for translational research, the inherent technical and biological variability of iPSC technologies remain a significant hurdle.[16,24] Disorders that reveal symptoms relatively late in adulthood, such as Parkinson's or Alzheimer's, are less likely to reveal early neurodevelopmental features. Therefore, it is important, at least in these latter models, to compare neurons of equivalent functional maturity, and efficient ways to identify electrophysiologically active neurons are needed. By revealing the molecular signature of highly functional states of differentiated neurons (AP Type 5), we have shown the possibility to predict functional profiles without the need of electrophysiological measurements. The ability to efficiently identify neurons in a specific functional state compensates for the heterogeneous proportion of functional neurons among cell lines and will strengthen comparative analysis in stem cell models of brain disorders. Ultimately, strategies to provide electrophysiologically homogeneous human neurons will assist large-scale drug screening, which can lead to the discovery of efficient treatments for neurological and psychiatric disorders.

CONFLICT OF INTEREST

The authors declare no conflict of interest.

ACKNOWLEDGMENTS

We are grateful to Elisabeth Santo and Sarah Marshall for help with the morphological reconstruction. We thank Gage lab members Bobbie Miller and Lynne Moore for preparation of viral vectors and Eunice Meija for immunohistochemistry. Thanks to Gage lab (Prattap Venepalli, Apua Paquola, Sara Linker, Son Pham) and Yeo lab (Olga Botvinnik) members for fruitful bioinformatics discussions

on single-cell transcriptomics. We thank Mary Lynn Gage for edits on the manuscript. This study was supported by grants from Ipsen Pharma, Annette C. Merle-Smith, The Leona M. and Harry B. Helmsley Charitable Trust Grant #2012-PG-MED002, Bob and Mary Jane Engman, the JPB Foundation, G Harold and Leila Y. Mathers Foundation, and NIH Grants MH095741 (to F.H.G.); also by a Fay/Frank Seed Grant from the Brain Research Foundation and NIH Grants NS075449, HG004659, HG007005 (to G.W.Y.). G.W.Y. is an Alfred P Sloan Research Fellow. This work was also supported by NSF Graduate Research Fellowship (to B.K.), the George E. Hewitt Foundation for Medical Research (to J.E.) the EMBO Long-term fellowship, the Bettencourt Schueller Foundation and the Philippe Foundation (B.N.J.) and the FP7 Marie Curie International Outgoing Fellowship for Career Development (to C.B.).

AUTHOR CONTRIBUTIONS

CB designed and analyzed all experiments and wrote the manuscript with input from GWY and FHG. MVDH and JE prepared the single-cell cDNA libraries and performed the cDNA QC. CB and BK analyzed the single-cell transcriptome data. BNJ, JB, AP and CB performed the FACS experiments. CB, MG, RVH and CM performed the patch-clamping experiments. TE, AP and CB performed the tissue culture. MK and AKB reconstructed the neuronal morphology. RJ designed the viral vector constructs.

REFERENCES

1 Greig LC, Woodworth MB, Galazo MJ, Padmanabhan H, Macklis JD. Molecular logic of neocortical projection neuron specification, development and diversity. *Nat Rev Neurosci* 2013; **14**: 755–769.
2 Molyneaux BJ, Arlotta P, Menezes JRL, Macklis JD. Neuronal subtype specification in the cerebral cortex. *Nat Rev Neurosci* 2007; **8**: 427–437.
3 Cho M-S, Hwang D-Y, Kim D-W. Efficient derivation of functional dopaminergic neurons from human embryonic stem cells on a large scale. *Nat Protoc* 2008; **3**: 1888–1894.
4 Vadodaria KC, Mertens J, Paquola A, Bardy C, Li X, Jappelli R *et al.* Generation of functional human serotonergic neurons from fibroblasts. *Mol Psychiatry* 2015; **21**: 49–61.
5 Shi Y, Kirwan P, Smith J, Robinson HPC, Livesey FJ. Human cerebral cortex development from pluripotent stem cells to functional excitatory synapses. *Nat Neurosci* 2012; **15**: 477–486.
6 Boyer LF, Campbell B, Larkin S, Mu Y, Gage FH. Dopaminergic differentiation of human pluripotent cells. *Curr Protoc Stem Cell Biol* 2012; **Chapter 1**: Unit1H.6.
7 Mertens J, Marchetto MC, Bardy C, Gage FH. Evaluating cell reprogramming, differentiation and conversion technologies in neuroscience. *Nat Rev Neurosci* 2016; **17**: 424–437.
8 Kirwan P, Turner-Bridger B, Peter M, Momoh A, Arambepola D, Robinson HPC *et al.* Development and function of human cerebral cortex neural networks from pluripotent stem cells *in vitro*. *Development* 2015; **142**: 3178–3187.
9 Wernig M, Zhao J-P, Pruszak J, Hedlund E, Fu D, Soldner F *et al.* Neurons derived from reprogrammed fibroblasts functionally integrate into the fetal brain and improve symptoms of rats with Parkinson's disease. *Proc Natl Acad Sci USA* 2008; **105**: 5856–5861.
10 Pang ZP, Yang N, Vierbuchen T, Ostermeier A, Fuentes DR, Yang TQ *et al.* Induction of human neuronal cells by defined transcription factors. *Nature* 2011; **476**: 220–223.
11 Chanda S, Ang CE, Davila J, Pak C, Mall M, Lee QY *et al.* Generation of induced neuronal cells by the single reprogramming factor ASCL1. *Stem Cell Reports* 2014; **3**: 282–296.
12 Zhang Y, Pak C, Han Y, Ahlenius H, Zhang Z, Chanda S *et al.* Rapid single-step induction of functional neurons from human pluripotent stem cells. *Neuron* 2013; **78**: 785–798.
13 Bardy C, Van den Hurk M, Eames T, Marchand C, Hernandez RV, Kellogg M *et al.* Neuronal medium that supports basic synaptic functions and activity of human neurons *in vitro*. *Proc Natl Acad Sciences* 2015; **112**: E2725–E2734.
14 Prilutsky D, Palmer NP, Smedemark-Margulies N, Schlaeger TM, Margulies DM, Kohane IS. iPSC-derived neurons as a higher-throughput readout for autism: promises and pitfalls. *Trends Mol Med* 2014; **20**: 91–104.
15 Belinsky GS, Moore AR, Short SM, Rich MT, Antic SD. Physiological properties of neurons derived from human embryonic stem cells using a dibutyryl cyclic AMP-based protocol. *Stem Cells Dev* 2011; **20**: 1733–1746.
16 Wu H, Xu J, Pang ZP, Ge W, Kim KJ, Blanchi B *et al.* Integrative genomic and functional analyses reveal neuronal subtype differentiation bias in human embryonic stem cell lines. *Proc Natl Acad Sci USA* 2007; **104**: 13821–13826.
17 Hu BY, Weick JP, Yu J, Ma LX, Zhang XQ, Thomson JA *et al.* Neural differentiation of human induced pluripotent stem cells follows developmental principles but with variable potency. *Proc Natl Acad Sci* 2010; **107**: 4335–4340.
18 Tang X, Zhou L, Wagner AM, Marchetto MC, Muotri AR, Gage FH *et al.* Astroglial cells regulate the developmental timeline of human neurons differentiated from induced pluripotent stem cells. *Stem Cell Res* 2013; **11**: 743–757.
19 Weick JP, Johnson MA, Skroch SP, Williams JC, Deisseroth K, Zhang S-C. Functional control of transplantable human ESC-derived neurons via optogenetic targeting. *Stem Cells* 2010; **28**: 2008–2016.
20 Yang N, Ng YH, Pang ZP, Südhof TC, Wernig M. Induced neuronal cells: how to make and define a neuron. *Cell Stem Cell* 2011; **9**: 517–525.
21 Geurts P, Ernst D, Wehenkel L. Extremely randomized trees. *Mach Learn* 2006; **63**: 3–42.
22 Marr RA, Guan H, Rockenstein E, Kindy M, Gage FH, Verma I *et al.* Neprilysin regulates amyloid Beta peptide levels. *J Mol Neurosci* 2004; **22**: 5–11.
23 Brennand KJ, Simone A, Jou J, Gelboin-Burkhart C, Tran N, Sangar S *et al.* Modelling schizophrenia using human induced pluripotent stem cells. *Nature* 2011; **473**: 221–225.
24 Dolmetsch R, Geschwind DH. The human brain in a dish: the promise of iPSC-derived neurons. *Cell* 2011; **145**: 831–834.
25 Shcheglovitov A, Shcheglovitova O, Yazawa M, Portmann T, Shu R, Sebastiano V *et al.* SHANK3 and IGF1 restore synaptic deficits in neurons from 22q13 deletion syndrome patients. *Nature* 2013; **503**: 267–271.
26 Wen Z, Nguyen HN, Guo Z, Lalli MA, Wang X, Su Y *et al.* Synaptic dysregulation in a human iPS cell model of mental disorders. *Nature* 2014; **515**: 414–418.
27 Lledo P-MM, Alonso M, Grubb MS. Adult neurogenesis and functional plasticity in neuronal circuits. *Nat Rev Neurosci* 2006; **7**: 179–193.
28 Trapnell C, Cacchiarelli D, Grimsby J, Pokharel P, Li S, Morse M *et al.* The dynamics and regulators of cell fate decisions are revealed by pseudotemporal ordering of single cells. *Nat Biotechnol* 2014; **32**: 381–386.
29 Tsetsenis T, Younts TJ, Chiu CQ, Kaeser PS, Castillo PE, Südhof TC. Rab3B protein is required for long-term depression of hippocampal inhibitory synapses and for normal reversal learning. *Proc Natl Acad Sci* 2011; **108**: 14300–14305.
30 Lewis S. Synaptic plasticity: a key player in presynaptic plasticity. *Nat Rev Neurosci* 2011; **12**: 548–548.
31 Pedrola L, Espert A, Wu X, Claramunt R, Shy ME, Palau F. GDAP1, the protein causing Charcot-Marie-Tooth disease type 4A, is expressed in neurons and is associated with mitochondria. *Hum Mol Genet* 2005; **14**: 1087–1094.
32 Lewis DA. The human brain revisited: opportunities and challenges in post-mortem studies of psychiatric disorders. *Neuropsychopharmacology* 2002; **26**: 143–154.
33 Moore AR, Filipovic R, Mo Z, Rasband MN, Zecevic N, Antic SD. Electrical excitability of early neurons in the human cerebral cortex during the second trimester of gestation. *Cereb Cortex* 2009; **19**: 1795–1805.
34 Moore AR, Zhou W-L, Jakovcevski I, Zecevic N, Antic SD. Spontaneous electrical activity in the human fetal cortex *in vitro*. *J Neurosci* 2011; **31**: 2391–2398.
35 Nicholas CR, Chen J, Tang Y, Southwell DG, Chalmers N, Vogt D *et al.* Functional maturation of hPSC-derived forebrain interneurons requires an extended timeline and mimics human neural development. *Cell Stem Cell* 2013; **12**: 573–586.
36 Vierbuchen T, Ostermeier A, Pang ZP, Kokubu Y, Südhof TC, Wernig M. Direct conversion of fibroblasts to functional neurons by defined factors. *Nature* 2010; **463**: 1035–1041.
37 Eberwine J, Sul J-Y, Bartfai T, Kim J. The promise of single-cell sequencing. *Nat Methods* 2014; **11**: 25–27.
38 Saliba A-E, Westermann AJ, Gorski SA, Vogel J. Single-cell RNA-seq: advances and future challenges. *Nucleic Acids Res* 2014; **42**: 8845–8860.
39 Sandberg R. Entering the era of single-cell transcriptomics in biology and medicine. *Nat Methods* 2014; **11**: 22–24.
40 Shapiro E, Biezuner T, Linnarsson S. Single-cell sequencing-based technologies will revolutionize whole-organism science. *Nat Rev Genet* 2013; **14**: 618–630.
41 Tang F, Barbacioru C, Wang Y, Nordman E, Lee C, Xu N *et al.* mRNA-Seq whole-transcriptome analysis of a single cell. *Nat Methods* 2009; **6**: 377–382.
42 Picelli S, Björklund ÅK, Faridani OR, Sagasser S, Winberg G, Sandberg R. Smart-seq2 for sensitive full-length transcriptome profiling in single cells. *Nat Methods* 2013; **10**: 1096–1098.
43 Wu AR, Neff NF, Kalisky T, Dalerba P, Treutlein B, Rothenberg ME *et al.* Quantitative assessment of single-cell RNA-sequencing methods. *Nat Methods* 2014; **11**: 41–46.
44 Islam S, Kjällquist U, Moliner A, Zajac P, Fan J-B, Lonnerberg P *et al.* Characterization of the single-cell transcriptional landscape by highly multiplex RNA-seq. *Genome Res* 2011; **21**: 1160–1167.
45 Islam S, Kjällquist U, Moliner A, Zajac P, Fan J-B, Lonnerberg P *et al.* Highly multiplexed and strand-specific single-cell RNA 5[prime] end sequencing. *Nat Protoc* 2012; **7**: 813–828.
46 Tang F, Barbacioru C, Nordman E, Li B, Xu N, Bashkirov VI *et al.* RNA-Seq analysis to capture the transcriptome landscape of a single cell. *Nat Protoc* 2010; **5**: 516–535.
47 Picelli S, Faridani OR, Björklund ÅK, Winberg G, Sagasser S, Sandberg R. Full-length RNA-seq from single cells using Smart-seq2. *Nat Protoc* 2014; **9**: 171–181.

48 Patel AP, Tirosh I, Trombetta JJ, Shalek AK, Gillespie SM, Wakimoto H *et al.* Single-cell RNA-seq highlights intratumoral heterogeneity in primary glioblastoma. *Science* 2014; **344**: 1396–1401.
49 Toriello NM, Douglas ES, Thaitrong N, Hsiao SC, Francis MB, Bertozzi CR *et al.* Integrated microfluidic bioprocessor for single-cell gene expression analysis. *Proc Natl Acad Sci* 2008; **105**: 20173–20178.
50 Belinsky GS, Rich MT, Sirois CL, Short SM, Pedrosa E, Lachman HM *et al.* Patch-clamp recordings and calcium imaging followed by single-cell PCR reveal the developmental profile of 13 genes in iPSC-derived human neurons. *Stem Cell Res* 2014; **12**: 101–118.
51 Faragó N, Kocsis AK, Lovas S, Molnár G, Boldog E, Rózsa M *et al.* Digital PCR to determine the number of transcripts from single neurons after patch-clamp recording. *BioTechniques* 2013; **54**: 327–336.
52 Toledo-Rodriguez M, Markram H. Single-cell RT-PCR, a technique to decipher the electrical, anatomical, and genetic determinants of neuronal diversity. *Methods Mol Biol* 2007; **403**: 123–139.
53 Toledo-Rodriguez M, Blumenfeld B, Wu C, Luo J, Attali B, Goodman P *et al.* Correlation maps allow neuronal electrical properties to be predicted from single-cell gene expression profiles in rat neocortex. *Cereb Cortex* 2004; **14**: 1310–1327.
54 Subkhankulova, Yano K, Hugh PC Robinson, Livesey FJ. Grouping and classifying electrophysiologically-defined classes of neocortical neurons by single cell, whole-genome expression profiling. *Front Mol Neurosci* 2010; **3**: 10.
55 Fuzik J, Zeisel A, Mate Z, Calvigioni D, Yanagawa Y, Szabo G *et al.* Integration of electrophysiological recordings with single-cell RNA-seq data identifies neuronal subtypes. *Nat Biotechnol* 2015; **34**: 175–183.
56 Cadwell CR, Palasantza A, Jiang X, Berens P, Deng Q, Yilmaz M *et al.* Electrophysiological, transcriptomic and morphologic profiling of single neurons using Patch-seq. *Nat Biotechnol* 2015; **34**: 199–203.
57 Steward O, Wallace CS, Lyford GL, Worley PF. Synaptic activation causes the mRNA for the IEG arc to localize selectively near activated postsynaptic sites on dendrites. *Neuron* 1998; **21**: 741–751.
58 Cajigas IJ, Tushev G, Will TJ, tom Dieck S, Fuerst N, Schuman EM. The local transcriptome in the synaptic neuropil revealed by deep sequencing and high-resolution imaging. *Neuron* 2012; **74**: 453–466.
59 Bassell GJ, Warren ST. Fragile X syndrome: loss of local mRNA regulation alters synaptic development and function. *Neuron* 2008; **60**: 201–214.
60 Bagni C, Greenough WT. From mRNP trafficking to spine dysmorphogenesis: the roots of fragile X syndrome. *Nat Rev Neurosci* 2005; **6**: 376–387.
61 Wichterle H, Gifford D, Mazzoni E. Mapping neuronal diversity one cell at a time. *Science* 2013; **341**: 725–726.
62 Markram H, Muller E, Ramaswamy S, Reimann MW, Abdellah M, Sanchez CA *et al.* Reconstruction and simulation of neocortical microcircuitry. *Cell* 2015; **163**: 456–492.
63 DeFelipe J, López-Cruz PL, Benavides-Piccione R, Bielza C, Larrañaga P, Anderson S *et al.* New insights into the classification and nomenclature of cortical GABAergic interneurons. *Nat Rev Neurosci* 2013; **14**: 202–216.
64 Gupta A, Wang Y, Markram H. Organizing principles for a diversity of GABAergic interneurons and synapses in the neocortex. *Science* 2000; **287**: 273–278.
65 Bardy C, Alonso M, Bouthour W, Lledo P-MM. How, when, and where new inhibitory neurons release neurotransmitters in the adult olfactory bulb. *J Neurosci* 2010; **30**: 17023–17034.
66 Carleton A, Petreanu LT, Lansford R, Alvarez-Buylla A, Lledo P-MM. Becoming a new neuron in the adult olfactory bulb. *Nat Neurosci* 2003; **6**: 507–518.
67 Markram H, Toledo-Rodriguez M, Wang Y, Gupta A, Silberberg G, Wu C. Interneurons of the neocortical inhibitory system. *Nat Rev Neurosci* 2004; **5**: 793–807.
68 Ascoli GA, Alonso-Nanclares L, Anderson SA, Barrionuevo G, Benavides-Piccione R, Burkhalter A *et al.* Petilla terminology: nomenclature of features of GABAergic interneurons of the cerebral cortex. *Nat Rev Neurosci* 2008; **9**: 557–568.
69 Druckmann S, Hill S, Schurmann F, Markram H, Segev I. A hierarchical structure of cortical interneuron electrical diversity revealed by automated statistical analysis. *Cerebral Cortex* 2013; **23**: 2994–3006.
70 Tasic B, Menon V, Nguyen TN, Kim T-K, Jarsky T, Yao Z *et al.* Adult mouse cortical cell taxonomy revealed by single cell transcriptomics. *Nat Neurosci* 2016; **19**: 335–346.
71 Hawrylycz M, Miller JA, Menon V, Feng D, Dolbeare T, Guillozet-Bongaarts AL *et al.* Canonical genetic signatures of the adult human brain. *Nat Neurosci* 2015; **18**: 1832–1844.
72 Stein JL, la Torre-Ubieta de L, Tian Y, Parikshak NN, Hernández IA, Marchetto MC *et al.* A quantitative framework to evaluate modeling of cortical development by neural stem cells. *Neuron* 2014; **83**: 69–86.
73 McConnell MJ, Lindberg MR, Brennand KJ, Piper JC, Voet T, Cowing-Zitron C *et al.* Mosaic copy number variation in human neurons. *Science* 2013; **342**: 632–637.
74 Bellin M, Marchetto MC, Gage FH, Mummery CL. Induced pluripotent stem cells: the new patient? *Nat Rev Mol Cell Biol* 2012; **13**: 713–726.
75 Marchetto MC, Brennand KJ, Boyer LF, Gage FH. Induced pluripotent stem cells (iPSCs) and neurological disease modeling: progress and promises. *Hum Mol Genet* 2011; **20**: R109–R115.
76 Paşca SP, Portmann T, Voineagu I, Yazawa M, Shcheglovitov A, Paşca AM *et al.* Using iPSC-derived neurons to uncover cellular phenotypes associated with Timothy syndrome. *Nat Med* 2011; **17**: 1657–1662.
77 Yu DX, Marchetto MC, Gage FH. Therapeutic translation of iPSCs for treating neurological disease. *Stem Cell* 2013; **12**: 678–688.
78 Marchetto MC, Carromeu C, Acab A, Yu D, Yeo GW, Mu Y *et al.* A model for neural development and treatment of Rett syndrome using human induced pluripotent stem cells. *Cell* 2010; **143**: 527–539.

Supplementary Information accompanies the paper on the *Molecular Psychiatry* website (http://www.nature.com/mp)